J. Fluid Mech. (1990), *vol.* 210, *pp.* 501–535
Printed in Great Britain

Frictional–collisional equations of motion for particulate flows and their application to chutes

By P. C. JOHNSON, P. NOTT AND R. JACKSON
Department of Chemical Engineering, Princeton University, Princeton, NJ 08544, USA

(Received 7 March 1988 and in revised form 4 July 1989)

Measurements of the relation between mass hold-up and flow rate have been made for glass beads in fully developed flow down an inclined chute, over the whole range of inclinations for which such flows are possible. Velocity profiles in the flowing material have also been measured. For a given inclination it is found that two different flow regimes may exist for each value of the flow rate in a certain interval. One is an 'energetic' flow, and is produced when the particles are dropped into the chute from a height, while the other is relatively quiescent and occurs when entry to the chute is regulated by a gate. At some values of the inclination jumps in the flow pattern occur between these branches, and it is even possible for both branches to coexist in the same chute, separated by a shock. A theoretical treatment of chute flow has been based on a rheological model of the material which takes into account both collisional and frictional mechanisms for generating stress. Its predictions include most aspects of the observed behaviour, but quantitative comparison of theory and experiment is difficult because of the uncertain values of some parameters appearing in the theory.

1. Introduction

Particulate flow behaviour is governed by interactions occurring at the microstructural, or particle level. For granular flows in which interstitial fluid effects are negligible the mechanical behaviour is determined entirely by the forces exerted at particle–particle contacts. For the case of slow deformation and high density, particles sustain contact as they slide relative to one another. Normal and tangential frictional forces at points of contact then dominate the flow behaviour. The rapid shearing of low-density particle assemblies, on the other hand, induces vigorous particle motions, contacts are of short duration, and momentum is transmitted when particles collide.

In the past most models of particulate flow behaviour assumed that one of the two limiting stress generation mechanisms, friction or collisions, dominated and governed the flow behaviour. Constitutive theories originating from soil mechanics (Coulomb 1776; Reynolds 1885; Drucker & Prager 1952; de Jong 1959; Schofield & Wroth 1968) focus on the slow deformation–high density limit. These descriptions of quasi-static motion are mostly empirical in nature and require much experimental data to characterize any material's behaviour. The opposite rapid shear–low density limit has been modelled more recently by the so-called 'kinetic grain theories' that draw analogies between high shear rate particulate motions and the movement of gas molecules (Jenkins & Savage 1983; Haff 1983; Lun *et al.* 1984; Jenkins & Richman 1985). The main difference from molecular motion is that particle–particle collisions

are inelastic. In this regime inertial effects are dominant and constitutive expressions are derived by following established procedures of the kinetic theory of dense gases. The collisional–kinetic constitutive expressions derived by this approach are related to physical properties of the material, such as the grain diameter and density, and to the 'grain temperature'. This new quantity, which is analogous to the thermodynamic temperature of a gas or liquid, is a measure of the kinetic energy of random motion of the particles.

Most flows of practical interest fall into the intermediate regime where both frictional contacts and particle–particle collisions are significant. As yet there are no established theories that describe the flow behaviour in these conditions. The frictional–collisional model proposed by Johnson & Jackson (1987) is a simplistic attempt to combine the available constitutive theories for rapid and slow deformation rate flows without introducing any new parameters. This model is at best an expedient awaiting the development of more fundamentally based theories, but it does allow one to investigate the relative roles of the two limiting stress mechanisms. It has been applied to the problem of horizontal plane shearing by Johnson & Jackson (1987), who compared its predictions with experimental observations in an annular shear cell.

Annular shear cells and inclined chute flows are the two flow geometries most suitable for comparison with theoretical predictions. Relatively detailed data from the former have been provided by Savage & Sayed (1984), but comparable data from inclined chute experiments are not available, though many studies have been reported (Augenstein & Hogg 1978; Savage 1978, 1979, 1983; Ishida & Shirai 1979; Brennen, Sieck & Paslaski 1983; Campbell, Brennen & Sabersky 1985; Patton, Brennen & Sabersky 1987). Unfortunately the information needed to compare these experimental observations with predictions of the theory is seldom provided; for example, the most recent work of Patton *et al.* is based on extensive measurements of flow rate, depth and mean density, but these are not reported directly, nor are the corresponding values of the chute inclination. In this paper we present predictions of flows down inclined planes, using the frictional–collisional model, and compare them with observations on an experimental chute. This case is an excellent example of the need for models that incorporate both of the limiting stress mechanisms. Calculations indicate that neither limiting model can predict much of the observed behaviour, while the experimental observations include behaviour not previously reported. The full model, while far from satisfactory as a quantitative predictor, has fair success in reproducing the overall pattern of observed behaviour.

2. Equations of motion and boundary conditions

2.1. *Governing equations*

In a previous paper (Johnson & Jackson 1987) the following equations for dry, cohesionless particulate flows were proposed:

$$\frac{\mathrm{D}\rho}{\mathrm{D}t} + \rho \nabla \cdot \boldsymbol{u} = 0, \tag{2.1}$$

$$\rho \frac{\mathrm{D}\boldsymbol{u}}{\mathrm{D}t} = \rho \boldsymbol{g} - \nabla \cdot (\boldsymbol{\sigma}_{\mathrm{f}} + \boldsymbol{\sigma}_{\mathrm{c}}), \tag{2.2}$$

$$\tfrac{3}{2}\rho \frac{\mathrm{D}T}{\mathrm{D}t} = -\nabla \cdot \boldsymbol{q}_{\mathrm{PT}} - \boldsymbol{\sigma}_{\mathrm{c}} : \nabla \boldsymbol{u} - I. \tag{2.3}$$

The first of these is the usual continuity equation in which ρ is the bulk density of solids and $\mathrm{D}/\mathrm{D}t$ denotes the material derivative. The momentum equation (2.2) reflects the assumption that the total stress in the granular continuum is the sum of frictional $\boldsymbol{\sigma}_\mathrm{f}$, and collisional–kinetic, $\boldsymbol{\sigma}_\mathrm{c}$, contributions, with each calculated independently from constitutive expressions derived for the limits of purely collisional and purely frictional interactions, respectively. In (2.2) $\boldsymbol{u}$ and $\boldsymbol{g}$ represent the mean velocity and specific body force. Because the collisional–kinetic constitutive expressions depend on the bulk density, rate of deformation and the grain temperature T, the balance equations for mass and momentum are supplemented by the 'pseudo-thermal energy equation' (2.3). This equation represents a local balance of pseudo-thermal energy ($=\frac{3}{2}\rho T$) between the flux divergence $\boldsymbol{\nabla}\cdot\boldsymbol{q}_\mathrm{PT}$, the rate of generation due to shearing $-\boldsymbol{\sigma}_\mathrm{c}:\boldsymbol{\nabla u}$, and the rate of dissipation/volume I due to inelastic collisions. The latter quantity depends on the particle–particle coefficient of restitution e_p. Inherent in the derivation of (2.3) is the postulate that frictional work generates true molecular internal energy (heat), and does not contribute to the generation of pseudo-thermal energy.

2.2. *Boundary conditions at solid and free surfaces*

For the situation where interactions between the particles and the boundary are entirely due to collisions boundary conditions were obtained by Hui *et al.* (1984) using heuristic arguments. Later Jenkins & Richman (1986) showed that the conditions could be derived more formally, using kinetic theory, provided that the boundary was endowed with a specific geometric structure, and their derivation revealed the omission of a physically important term from the conditions of Hui *et al.* Neither of these works addressed the case of interest here, where both frictional and collisional interactions are important, but Johnson & Jackson (1987) derived boundary conditions for this case using arguments similar to those employed by Hui *et al.* (1984). For the limiting situation in which collisional effects dominate, these conditions reduce to the same form as those of Jenkins & Richman, but with certain parameters to be determined by measurement since the boundary geometry is not invoked explicitly. In the present work the conditions of Johnson & Jackson will be used and a sketch of their derivation follows.

By equating the stress exerted by flowing particles on a solid boundary with the limit of the stress in the material on approaching the boundary, the following condition on the slip velocity results:

$$\frac{\boldsymbol{u}_\mathrm{sl}\cdot(\boldsymbol{\sigma}_\mathrm{f}+\boldsymbol{\sigma}_\mathrm{c})\cdot\boldsymbol{n}}{|\boldsymbol{u}_\mathrm{sl}|}+\frac{\phi'\sqrt{3\pi}\rho_\mathrm{p}\nu T^{\frac{1}{2}}|\boldsymbol{u}_\mathrm{sl}|}{6\nu_0[1-(\nu/\nu_0)^{\frac{1}{3}}]}+N_\mathrm{f}\tan\delta=0. \tag{2.4}$$

Here the slip velocity, $\boldsymbol{u}_\mathrm{sl}=\boldsymbol{u}-\boldsymbol{u}_\mathrm{wall}$, is the relative velocity between the wall and particles in contact with it, while $\boldsymbol{n}$ is the unit normal vector directed from the boundary into the material. The solids volume fraction is denoted by ν, which is related to the bulk density of solids ρ and the density of a single particle ρ_p by $\rho=\rho_\mathrm{p}\nu$. The solids volume fraction for a random close packing is represented by ν_0, and in this work it is assigned the value 0.65. The first term in (2.4) represents the limit of the stress in the material on approaching the boundary, while the second and third terms represent the stress acting on the boundary due to particle–wall collisions and friction, respectively. The former is proportional to a 'specularity coefficient', ϕ', which is defined to be the average fraction of relative tangential momentum transferred in a particle–boundary collision. Its value depends on the large-scale

roughness of the surface and varies between zero for perfectly specular collisions and unity for perfectly diffuse collisions. The magnitude of the tangential frictional contribution to the stress is assumed to be $N_f \tan\delta$, where N_f is the normal frictional component of stress and δ is the angle of friction between the surface and the particulate material.

From an energy balance on a slice of vanishingly small thickness enclosing an element of the solid boundary, the following condition can also be derived:

$$-\boldsymbol{n}\cdot\boldsymbol{q}_{PT} = \mathscr{D} + \boldsymbol{u}_{sl}\cdot\boldsymbol{S}_c^b. \tag{2.5}$$

Equation (2.5) is a statement that the flux of pseudo-thermal energy to the boundary equals the difference between the rate of pseudo-thermal energy dissipation/area due to inelastic particle-wall collisions, $\mathscr{D}$, and the rate of energy generation that occurs as particles slip along the boundary. $\boldsymbol{S}_c^b$ is the force per unit area on the boundary due to grain–boundary collisions, as given by the second term on the left-hand side of (2.4). $\boldsymbol{u}_{sl}\cdot\boldsymbol{S}_c^b$ is inherently negative and represents a production of pseudo-thermal energy. An expression for $\mathscr{D}$ proposed by Johnson & Jackson (1987) is

$$\mathscr{D} = [\tfrac{1}{4}\pi\rho_p d^3 T(1-e_w^2)]\left[\frac{(3T)^{\frac{1}{2}}}{d[(\nu_0/\nu)^{\frac{1}{3}}-1]}\right]\left[\frac{1}{d^2(\nu_0/\nu)^{\frac{2}{3}}}\right], \tag{2.6}$$

where e_w is the particle–wall coefficient of restitution.

For flows involving free surfaces, additional stress and pseudo-thermal energy boundary conditions are needed. A pseudo-thermal energy balance on an infinitely thin control region at the surface indicates that the flux of pseudo-thermal energy must vanish, so

$$\boldsymbol{n}\cdot\boldsymbol{q}_{PT} = 0. \tag{2.7}$$

There are two approaches to developing a stress condition at the free surface. The first is to adopt the traditional stress-free surface conditions:

$$\boldsymbol{n}\cdot\boldsymbol{n}\cdot(\boldsymbol{\sigma}_f+\boldsymbol{\sigma}_c) = 0 \tag{2.8}$$

and

$$\boldsymbol{n}\cdot\boldsymbol{t}\cdot(\boldsymbol{\sigma}_f+\boldsymbol{\sigma}_c) = 0 \tag{2.9}$$

which require the total normal (2.8) and tangential (2.9) stresses acting at the free surface to vanish. (Here $\boldsymbol{t}$ denotes a unit vector in the direction of flow.) However, these give rise to difficulties unless the free surface is at infinity, since the numerical results indicate that the stress retains quite large values to within a fraction of a particle diameter of the nominal free surface, after which it drops rapidly to zero. This is physically unrealistic and also introduces a stiffness problem in the numerical solution. An alternative approach is to recognize the discrete nature of the particulate material by writing a force balance on the particles in the layer adjacent to the free surface:

$$\tfrac{1}{6}\pi\rho_p d^3\boldsymbol{g} = \boldsymbol{n}\cdot(\boldsymbol{\sigma}_f+\boldsymbol{\sigma}_c)\,a_c(\nu), \tag{2.10}$$

where $a_c(\nu)$, the area occupied per particle, is given (Johnson & Jackson 1987) by

$$a_c(\nu) = d^2(\nu_0/\nu)^{\frac{2}{3}}. \tag{2.11}$$

When (2.10) is combined with (2.11) and constitutive expressions are specified for $\boldsymbol{\sigma}_f$ and $\boldsymbol{\sigma}_c$, it provides conditions on the total shear and normal stress at the free surface.

In writing (2.10) we recognize that each particle in the uppermost layer has a non-vanishing weight that must be supported. Though this seems reasonable for flowing layers with sharply defined surfaces, at small flow rates, where the density is very

low, our experiments show that the upper surface is quite diffuse and the physical relevance of (2.10) is then less clear. A more satisfactory approach to the free surface will be presented below in §5, but this has been used for only a limited number of cases as the computations are much slower and more expensive than those based on (2.10).

2.3. *Constitutive theory*

As in Johnson & Jackson (1987) we adopt existing constitutive expressions for $\boldsymbol{\sigma}_f$, $\boldsymbol{\sigma}_c$, $\boldsymbol{q}_{PT}$, and I. Recently, the development of collisional constitutive expressions has been the goal of many theoretical studies (Savage & Jeffrey 1981; Jenkins & Savage 1983; Lun *et al.* 1984; Jenkins & Richman 1985). Most derivations follow the framework developed for gas kinetic theories, and hence all are very similar. While all theories include the limit of high particle densities, only the expressions presented by Lun *et al.* (1984) are supposed to be applicable over the entire range of solids volume fractions. A slightly modified form of their constitutive expressions is as follows:

$$\boldsymbol{\sigma}_c = [\rho_p \nu T(1+4\eta\nu g_0) - \eta\mu_b \nabla\cdot\boldsymbol{u}]\boldsymbol{I} - \tfrac{1}{3}(2+\alpha)\left\{\frac{2\mu}{\eta(2-\eta)g_0}(1+\tfrac{8}{5}\eta\nu g_0)[1+\tfrac{8}{5}\eta(3\eta-2)\nu g_0]+\tfrac{6}{5}\mu_b\eta\right\}\boldsymbol{S} \quad (2.12)$$

$$\boldsymbol{q}_{PT} = \frac{-\lambda}{g_0}\left\{(1+\tfrac{12}{5}\eta\nu g_0)[1+\tfrac{12}{5}\eta^2(4\eta-3)\nu g_0]+\frac{64}{25\pi}(41-33\eta)(\eta\nu g_0)^2\right\}\nabla T - \frac{\lambda}{g_0}(1+\tfrac{12}{5}\eta\nu g_0)\tfrac{12}{5}\eta(2\eta-1)(\eta-1)\frac{\mathrm{d}}{\mathrm{d}\nu}(\nu^2 g_0)\frac{T}{\nu}\nabla\nu, \quad (2.13)$$

$$I = \frac{48}{\pi^{\frac{1}{2}}}\eta(1-\eta)\frac{\rho_p\nu^2}{d}g_0 T^{\frac{1}{2}}. \quad (2.14)$$

Here $\boldsymbol{S}$ is the deviatoric part of the rate of deformation tensor, and

$$\eta = \tfrac{1}{2}(1+e_p), \quad \mu = \frac{5m(T/\pi)^{\frac{1}{2}}}{16d^2}, \quad \lambda = \frac{75m(T/\pi)^{\frac{1}{2}}}{8\eta(41-33\eta)d^2}, \quad \mu_b = \frac{256\mu\nu^2 g_0}{5\pi}, \quad (2.15)$$

where m is the mass of a single particle, d the particle diameter, ρ_p the density of a single particle, and e_p denotes the coefficient of restitution for particle–particle collisions. Equations (2.12)–(2.15) are the same as the expressions derived by Lun *et al.* (1984) except for the multiplicative factor $\frac{1}{3}(2+\alpha)$ appearing in front of the deviatoric part of $\boldsymbol{\sigma}_c$. α is a constant of order unity that appears in expressions derived earlier by Jenkins & Savage (1983), but was eliminated in the analysis of Lun *et al.* It is a measure of the anisotropy of the distribution of collisions on a sphere in a shear field, and it is convenient to reintroduce it here as an adjustable parameter that must tend to unity when $e_p \to 1$ and $\nu \to 0$, for consistency with the kinetic theory of dilute gases. The second modification to the constitutive expressions of Lun *et al.* is the replacement of the Carnahan–Starling form of the radial distribution function $g_0(\nu)$ by

$$g_0 = \frac{1}{1-(\nu/\nu_0)^{\frac{1}{3}}}, \quad (2.16)$$

which ensures that $g_0 \to \infty$ when $\nu \to \nu_0$, and hence constrains the solids volume fraction to remain less than the close-packed value ν_0.

Most of our calculations were actually performed with the term in $\nabla\nu$ omitted from

(2.13). This term, which generates a pseudo-thermal energy flux proportional to the gradient of particle concentration, contains a factor $(\eta-1)$ which is always negative, so it predicts a physically unreasonable flux in the direction of increasing density! However, the numerical results are almost unaffected by inclusion or exclusion of this term, and this points to the source of the difficulty. The constitutive relations are approximations valid only when particle–particle collisions are almost elastic, and this term can be shown to represent a contribution to the energy flux of higher order in the inelasticity than the remaining terms. Indeed, to the same order of approximation as it can be neglected, η can be replaced by unity in the remaining terms, and direct calculation again confirms that the results are only slightly changed.

Constitutive theories for the frictional stress are empirical in nature and depend on quantities not directly related to physical characteristics of the grains such as the particle size, or surface roughness. The theories proposed by de Jong (1959, 1977) and Mandel (1947) assume that deformation is a superposition of rotations and plane shears on surfaces where the ratio of frictional shear stress S_f to frictional normal stress N_f reaches a prescribed value. The bulk density changes induced by yielding and shearing are not inherent features of these theories, but they are accounted for in the 'critical-state' theory developed by Drucker & Prager (1952), Roscoe, Schofield & Wroth (1958), Schofield & Wroth (1968), and Roscoe (1970).

For the case of steady plane shear flows treated here we are fortunate not to have to choose between the available theories, as all reduce to the Coulomb relationship between the frictional shear, S_f, and normal, N_f, stresses:

$$S_f = N_f \sin\phi, \tag{2.17}$$

where ϕ is the 'internal angle of friction', a quantity measured in slow plane shearing experiments. (Note that some authors prefer to define ϕ by the relationship $S_f = N_f \tan\phi$ so some care should be exercised when comparing various values of ϕ from the literature.)

Experimental observations indicate that the frictional normal stress increases rapidly with bulk density and diverges as the close-packed bulk density ν_0 is approached. A simple algebraic representation of this behaviour is

$$\begin{aligned} N_f(\nu) &= Fr\frac{(\nu-\nu_{\min})^p}{(\nu_0-\nu)^n} \quad (\nu > \nu_{\min}) \\ &= 0 \qquad\qquad\qquad (\nu \leqslant \nu_{\min}), \end{aligned} \tag{2.18}$$

where Fr, n, and p are constants. Frictional behaviour at low values of ν has yet to be observed so we assume that frictional interactions no longer occur at values of $\nu < \nu_{\min}$ for which evenly distributed particles no longer touch. Equations (2.17) and (2.18) are the constitutive expressions for the frictional contribution to the total stress, and we assume that they remain valid for more rapid deformations in which collisional interactions also contribute to the total stress.

3. Theory of fully developed flow down an inclined plane

The inclined chute serves as an important component of many industrial solids transport processes and flow down inclined planes is of geological interest. Accordingly, many investigators have studied this system (Augenstein & Hogg 1978; Campbell *et al.* 1985; Patton *et al.* 1987), some focusing on interesting and unusual behaviour such as 'granular jumps' (Brennen *et al.* 1983). In this study as in other

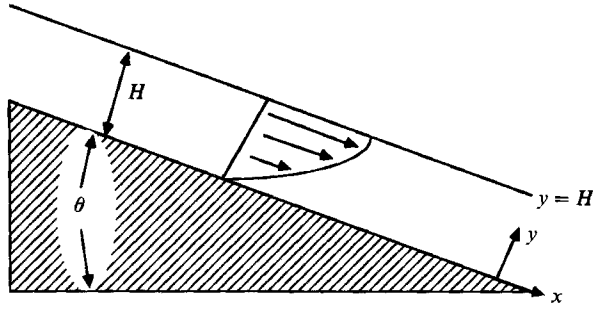

FIGURE 1. Inclined-plane shear flow.

investigations (Savage 1978, 1979, 1983; Ishida & Shirai 1979; Hutter & Scheiwiller 1983) the inclined chute is used to obtain flow measurements that are compared with predictions of constitutive theories.

3.1. *Equations of motion*

In the following analysis gravity-driven flow down an inclined chute is modelled by the steady, fully developed flow depicted in figure 1. The flow properties depend only on the coordinate y normal to the plane of shear. Our objective is to predict the dependence of the mass flow rate and the flow variables u, T, and ν on the inclination angle θ, flow depth H, and physical properties of the boundary and the grains. For this flow the continuity equation (2.1) is identically satisfied, while the two components of the momentum equation (2.2) and the pseudo-thermal energy equation (2.3) reduce to

$$0 = \frac{\partial}{\partial Y}[f_1(\nu)\,T^* + N_f^*(\nu)] + A\nu, \tag{3.1}$$

$$0 = \frac{\partial}{\partial Y}\left[\frac{f_2(\nu)\,T^{*\frac{1}{2}}}{A^{\frac{1}{2}}B^{\frac{1}{2}}}\frac{\partial u^*}{\partial Y} + \frac{N_f^*(\nu)\sin\phi}{B}\right] + A\nu, \tag{3.2}$$

$$0 = \frac{\partial}{\partial Y}\left[f_3(\nu)\,T^{*\frac{1}{2}}\left(\frac{\partial T^*}{\partial Y}\right) + f_4(\nu)\,T^{*\frac{3}{2}}\left(\frac{\partial \nu}{\partial Y}\right)\right] + ABf_2(\nu)\,T^{*\frac{1}{2}}\left(\frac{\partial u^*}{\partial Y}\right)^2 - A^2 f_5(\nu)\,T^{*\frac{3}{2}}. \tag{3.3}$$

The boundary conditions (2.4) and (2.5) apply at $Y = 0$ and take the following explicit form:

$$\frac{f_2(\nu)\,T^{*\frac{1}{2}}}{A^{\frac{1}{2}}B^{\frac{1}{2}}}\left(\frac{\partial u^*}{\partial Y}\right) + \frac{N_f^*(\nu)\sin\phi}{B} = \left(\frac{A}{B}\right)^{\frac{1}{2}}\phi' f_2(\nu) f_8(\nu)\,T^{*\frac{1}{2}}u^* + \frac{N_f^*(\nu)\tan\delta}{B} \tag{3.4}$$

and

$$\frac{\partial T^*}{\partial Y} = -\frac{f_4(\nu)}{f_3(\nu)}T^*\left(\frac{\partial \nu}{\partial Y}\right) + ACf_6(\nu)\,T^* - A^2BDf_7(\nu)\,u^{*2}. \tag{3.5}$$

At $Y = 1$ the condition (2.7) reduces to

$$\frac{\partial T^*}{\partial Y} = -\frac{f_4(\nu)}{f_3(\nu)}T^*\left(\frac{\partial \nu}{\partial Y}\right) \tag{3.6}$$

while the two components of (2.10), combined with (2.11), give

$$f_1(\nu)\,T^* + N_f^*(\nu) = \tfrac{1}{6}\pi\left[\frac{\nu(Y=1)}{\nu_0}\right]^{\frac{2}{3}} \tag{3.7}$$

$$f_1(\nu) = \nu[1+4\eta\nu g_0(\nu)],$$

$$f_2(\nu) = \tfrac{1}{3}(2+\alpha)\left(\frac{5\pi^{\frac{1}{2}}}{96}\right)\left\{\frac{[1+\frac{8}{5}\eta\nu g_0(\nu)][1+\frac{8}{5}\eta(3\eta-2)\,\nu g_0(\nu)]}{\eta(2-\eta)\,g_0(\nu)}+\frac{768\eta\nu^2 g_0(\nu)}{25\pi}\right\},$$

$$f_3(\nu) = \frac{25\pi^{\frac{1}{2}}}{16\eta(41-33\eta)}\left\{\left[\frac{1}{g_0}+\frac{12}{5}\eta\nu\right][1+\tfrac{12}{5}\eta^2(4\eta-3)\,\nu g_0]+\frac{64(41-33\eta)\,\eta^2\nu^2 g_0}{25\pi}\right\},$$

$$f_4(\nu) = \frac{25\pi^{\frac{1}{2}}}{16\eta(41-33\eta)}\left\{\left[\frac{1}{\nu g_0(\nu)}+\tfrac{12}{5}\eta\right][\tfrac{12}{5}\eta(2\eta-1)\,(\eta-1)]\frac{\partial\nu^2 g_0}{\partial\nu}\right\},$$

$$f_5(\nu) = \frac{48}{\pi^{\frac{1}{2}}}\eta(1-\eta)\,\nu^2 g_0(\nu), \quad f_6(\nu) = \frac{\pi\sqrt{3}\nu g_0(\nu)}{4\nu_0 f_3(\nu)},$$

$$f_7(\nu) = \frac{\pi\nu g_0(\nu)}{2\sqrt{3}\nu_0 f_3(\nu)}, \quad f_8(\nu) = \frac{\pi\nu g_0(\nu)}{2\sqrt{3}\nu_0 f_2(\nu)}$$

TABLE 1. Dimensionless functions

and
$$\frac{f_2(\nu)\,T^{*\frac{1}{2}}}{A^{\frac{1}{2}}B^{\frac{1}{2}}}\frac{\partial u^*}{\partial Y}+\frac{N_{\mathrm{f}}^*(\nu)\sin\phi}{B} = \tfrac{1}{6}\pi\left[\frac{\nu(Y=1)}{\nu_0}\right]^{\frac{2}{3}}. \tag{3.8}$$

Here the dimensionless mean velocity u^*, grain temperature T^*, spatial coordinate Y, and frictional normal stress $N_{\mathrm{f}}^*(\nu)$ are defined by

$$Y = \frac{y}{H}, \quad u^* = \frac{u}{(gH\sin\theta)^{\frac{1}{2}}}, \quad T^* = \frac{T}{gd\cos\theta}, \quad N_{\mathrm{f}}^*(\nu) = \frac{N_{\mathrm{f}}(\nu)}{\rho_{\mathrm{p}}\,gd\cos\theta} \tag{3.9}$$

and the dimensionless parameters A, B, C, and D are given by

$$A = \frac{H}{d}, \quad B = \tan\theta, \quad C = (1-e_{\mathrm{w}}^2), \quad D = \phi', \tag{3.10}$$

while the dimensionless functions $f_1(\nu)$ to $f_8(\nu)$ are defined in table 1 and depend on the solids volume fraction ν as well as the grain–grain coefficient of restitution e_{p}, through the associated variable $\eta = \frac{1}{2}(1+e_{\mathrm{p}})$.

At high bulk densities (3.1), (3.2), and boundary condition (3.4) are strictly valid only when $\tan\theta \geqslant \sin\phi \geqslant \tan\delta$. This is because the y-momentum equation (3.1) predicts that the total normal stress on any constant Y-plane, $N^*(Y)$, equals $N_{\mathrm{f}}^*(\nu)$ when frictional stresses dominate. The total driving shear stress is $N^*(Y)\tan\theta$ while the restraining force given by (3.2) is $N_{\mathrm{f}}^*(Y)\sin\phi$ in the frictional limit. Then if $\sin\phi > \tan\theta$ the equations predict flow against gravity because $\partial u^*/\partial Y < 0$ to satisfy (3.1) and (3.2). Thus, when finding solutions to (3.1)–(3.6), we must remember to restrict the frictional shear stress within the grains and at the boundary to values that at most equal the driving force. In these situations the flow is said to be 'locked' because $\partial u^*/\partial Y = 0$.

As noted earlier, in most of our calculations the constitutive relations were simplified in a way that replaces $f_4(\nu)$ by zero, thus eliminating the term in $\partial\nu/\partial Y$ from (3.3), with negligible effect on the computed results. In some of the calculations we will also omit the first term of the expression for $f_1(\nu)$ given in table 1, thus replacing it with

$$f_1(\nu) = 4\eta\nu^2 g_0(\nu).$$

Physically this is equivalent to neglecting the kinetic contribution to the particle pressure. When the density of the material is high this would be expected to make little difference, since the collisional contribution dominates. At low densities, on the other hand, Lun *et al.* (1984) showed that the kinetic contribution leads to a prediction that the normal stress in plane shear increases without bound as the concentration of the particles tends to zero. While this may be formally correct in an unbounded medium it is unrealistic for layers of the thickness considered here, since the increase in stress occurs at concentrations where the mean free path length is comparable with or longer than the total depth of the layer in question. However, at low flow rates the total depth of the flowing layer is observed to be a small multiple of the mean spacing between particle centres, while this in turn is several times the particle diameter. In these circumstances a significant fraction of all collisions involve a particle and the base of the chute, rather than a pair of particles. The situation is analogous to the transition region between bulk flow and Knudsen streaming for a gas, and this is notoriously intractable to theory. Nevertheless, the bounding of the thin, low-density layer by a solid surface will certainly prevent the development of the very large stresses generated by the kinetic contribution in an infinite medium. The device of simply ignoring the kinetic contribution to particle pressure does not provide an adequate treatment of this case, but it suppresses the divergence of the stress at low concentrations, and other difficulties which arise from it (Johnson 1987). We shall refer to this modification as the theory 'with $p_k = 0$'. When this simplification is used the corresponding results using the full constitutive relations are also presented for comparison.

3.2. *Numerical solution*

As a preliminary to numerical solution, (3.1) and (3.2) are integrated between values Y and 1 for the independent variable. After invoking the boundary conditions (3.7) and (3.8) this gives

$$f_1(\nu)\,T^* + N_f^*(\nu) = A\int_Y^1 \nu\,\mathrm{d}Y + \tfrac{1}{6}\pi\left[\frac{\nu(Y=1)}{\nu_0}\right]^{\frac{2}{3}} \tag{3.11}$$

and

$$\frac{f_2(\nu)\,T^{*\frac{1}{2}}}{A^{\frac{1}{2}}B^{\frac{1}{2}}}\frac{\partial u^*}{\partial Y} + \frac{N_f^*(\nu)\sin\phi}{B} = A\int_Y^1 \nu\,\mathrm{d}Y + \tfrac{1}{2}\pi\left[\frac{\nu(Y=1)}{\nu_0}\right]^{\frac{2}{3}}. \tag{3.12}$$

Using these equations the boundary condition (3.4) can be replaced by the following form, which gives the slip velocity directly:

$$u^* = \frac{[\tan\theta - \tan\delta]N_f^*(\nu)}{A^{\frac{1}{2}}B^{\frac{1}{2}}Df_2(\nu)\,T^{*\frac{1}{2}}} + \frac{B^{\frac{1}{2}}f_1(\nu)\,T^{*\frac{1}{2}}}{A^{\frac{1}{2}}Df_2(\nu)f_8(\nu)} \quad \text{at} \quad Y = 0. \tag{3.13}$$

The equations of motion are now (3.3), (3.11) and (3.12), while the associated boundary conditions are (3.5) and (3.13) at $Y = 0$, and (3.6) at $Y = 1$.

A numerical solution is initiated by specifying initial approximate forms for $u^*(Y)$ and $T^*(Y)$, then calculating a corresponding density profile $\nu(Y)$ from (3.11). The above equations and boundary conditions are then linearized about these approximate forms, N equally spaced grid points (including $Y = 0$ and $Y = 1$) are introduced, finite-difference approximations are substituted for the derivatives, and the integrals are approximated by the trapezium rule. The variable ν is replaced by the initial approximation above, wherever it appears, yielding $2N$ linear equations in the unknown values of u^* and T^* at the grid points. The solution of these provides a new initial approximation, and the process described can be iterated. In practice

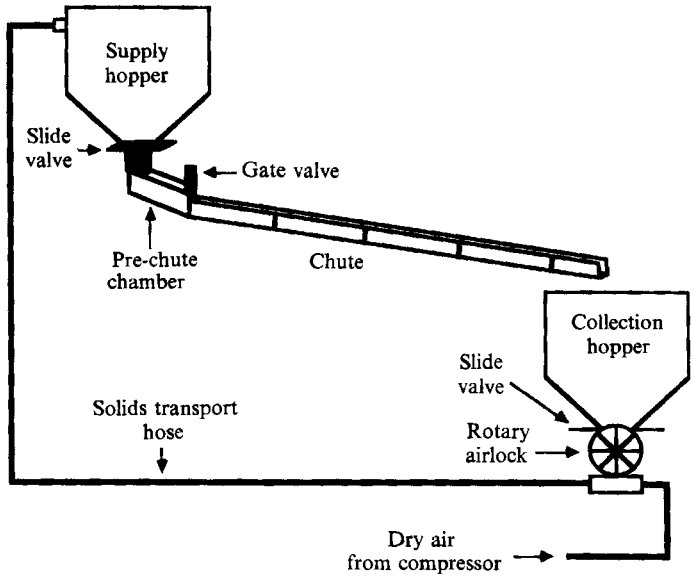

FIGURE 2. Schematic of the experimental chute.

it is found that convergence is better if some linear combination of the old and new approximations (typically 80% of the old and 20% of the new) is used to initiate the next iteration, rather than the new approximation itself. Iterations are continued until changes in the variables are everywhere less than 0.01% of their absolute values. Experiments with different numbers of grid points indicate that increases beyond 81 have little influence on the solutions, and this was the number used in most of the work reported.

A more detailed account of the computations is given by Johnson (1987), but before discussing the results we will describe our experimental observations.

4. Experiments with an inclined chute

Although many studies have reported the observed flow behaviour of particulate materials in chutes (Savage 1978, 1979, 1983; Augenstein & Hogg 1978; Ishida & Shirai 1979; Brennen *et al.* 1983; Hutter & Scheiwiller 1983; Campbell *et al.* 1985; Patton *et al.* 1987), none of them is complete enough to provide a useful comparison with theoretical predictions. In particular, none of the authors investigated the effect of varying the entrance conditions. In conjunction with our theoretical study, therefore, an experimental study was undertaken.

4.1. *Experimental apparatus*

Figure 2 is a schematic of the inclined chute flow loop. This consists of an upper supply hopper which feeds the chute through a pre-chute chamber. The particulate material flows down the chute into a collection hopper, which is equipped with a rotary airlock that feeds the material into a pneumatic transport line for return to the supply hopper. The system, when operated in a continuous fashion, has a maximum circulation rate of about 1.4 kg/s, limited by the capacity of the pneumatic transport system. The advantage of this system over those used by previous investigators (with the exception of Patton *et al.*) is that steady flows can

be maintained for indefinite time periods. Previous investigators were often limited to experiments less than a minute in duration.

The flow channel is 1.4 m long and 6.35 cm wide, and is bounded by vertical glass walls 12.7 cm high. For the purpose of this study the base of the chute was lined with a smooth aluminium plate that could be removed and covered with different grades of sandpaper, thus varying its roughness. In the present work the base plate was either unlined, or lined with a layer of 160-grit sandpaper. These configurations will be referred to as the smooth chute and the rough chute, respectively.

All the measurements reported here were made on a sample of 0.10 cm diameter glass beads. These were chosen because of the relatively high uniformity of material that could be obtained commercially. The diameters of the particles were specified by the manufacturer to vary from the mean by less than 10%. Physical characteristics of the beads will be discussed in §4.3.

Mass flow rates were measured by weighing the amount of material leaving the chute over a short time interval. The flow depth was defined as the greatest distance above the chute base at which particles were observed to collide with an inserted impact plate. Flow depths measured in this way represent the maximum height above the base achieved by any particles in the flow. The mass hold-up m_T in the flowing layer, per unit area of the base plate, was measured by the method customary in work on two-phase flow, namely the isolation of a known length of the flowing layer by barriers inserted upstream and downstream, rapidly and simultaneously. To accomplish this a rectangular box, of width equal to that of the channel, was pushed quickly into the flow with its open face downward. When this reached the base plate of the chute the material within it was trapped, and could be weighed after draining the rest of the material from the chute. In this way the weight of a section of the flowing layer about 7 cm long was found. The ratio of m_T to the flow depth, gives the average bulk density within the flow. In addition to these measurements, velocity profiles were measured with fibre-optic probes, of the type described by Patrose & Caram (1982), located at 31 cm intervals from the chute entrance. These probes were also used to measure free-surface velocities along the chute. This information, together with values of m_T and the depth of the layer at various positions, was valuable in determining whether or not flows had become fully developed before leaving. Details of the construction, calibration, and use of the fibre-optic velocity probes can be found in Johnson (1987), where there is also a more complete account of the experimental apparatus.

In chute experiments it is very important that θ be measured as accurately as possible, since a change in inclination of only 0.5° can have a dramatic effect on the flow behaviour. In our experiments θ was measured by a clinometer attached to the chute. This instrument, which was constructed from a precision protractor and sensitive bubble level, was accurate to within 0.05°. Uncertainties in other measurements were estimated at $\pm 5\%$ for the mass flow rate and the mass hold-up per unit base area, and $\pm 10\%$ for the velocity measurements.

Uncertainties in the measurement of the depth depend on the nature of the flow. High-density flows, $\nu \approx 0.60$, have distinct free surfaces and H can easily be measured to within the particle diameter. The concept of depth of the flowing layer is then well defined and the mean density, calculated as the ratio of m_T to H, is also a useful concept, since the density appears to be uniformly high throughout the layer. At low flow rates, on the other hand, the density of the layer is very small, and can be seen to vary markedly with depth, while the upper surface of the flowing material is quite diffuse. The frequency of collisions with the impact plate used to locate the 'free

surface' decreases gradually as the plate is raised, and there is no sharply identifiable 'surface'. Typically, at the lowest feed rates used, the mean value of the volume fraction solids, based on a 'depth' measured by the impact plate, is about 0.02. This corresponds to a mean spacing between particle centres of about three times the particle diameter, while the overall depth is only about six times this spacing. The concept of a flowing layer with a well-defined free surface and a meaningful mean density is then quite inappropriate: instead the particles move as a diffuse cloud whose density decreases continuously to zero with increasing height above the base plate. In these circumstances m_T is still a well-defined, measurable quantity, but the customary decomposition of this into factors representing a depth and a mean density is pointless and misleading. Since our experiments cover the whole range of behaviour from that just described to dense flowing layers with sharp surfaces, we choose to present our results as the relation between the flow rate and m_T, rather than H, since m_T is always well defined and measurable.

A key component of the flow loop is the pre-chute chamber which connects the supply hopper with the chute entrance. It is this portion of the apparatus that enables us to control the state of the particulate material as it enters the chute. In figure 2 there is seen to be a slide valve at the exit from the supply hopper, and also a gate valve at the exit from the pre-chute chamber onto the chute proper. By closing the gate valve and opening the slide valve the pre-chute chamber can be filled with beads. If the gate valve is then opened, the material enters the chute in a dense, slowly moving state. For these 'dense entry condition flows', in which the slide valve remains open, the mass flux into the chute is controlled by the gate valve. In an alternative mode of operation the gate valve is left fully open and the flow is controlled by manipulating the slide valve. The beads leaving the hopper then fall freely a distance of 30 cm onto the base of the pre-chute chamber. This drop, and subsequent bouncing off the base, generates a low density, highly energetic state at the chute entrance, and the resulting flows will be referred to as 'loose entry condition flows'.

4.2. *Experimental observations*

Measurements were made by setting the slope of the chute and the openings of the valves that control the flow, then determining the depth H of the flowing layer, its mass hold-up m_T, and the mass flow rate m per unit width of the chute. Velocity profiles were also measured for a number of cases. Results are presented as plots of $\dot{m}^*$ *vs.* m_T^*, for a sequence of values of the chute inclination ranging from the smallest slope at which the material will flow, to a slope at which it continues to accelerate down the whole available length. Here $\dot{m}^*$ denotes a dimensionless mass flow rate defined by $\dot{m}^* = \dot{m}/\rho_p d(gd)^{\frac{1}{2}}$, and m_T^* is a dimensionless mass hold-up defined by $m_T^* = m_T/\rho_p d$. Measurements for the smooth chute base are plotted in figures 4–9, while corresponding results for the rough chute base can be found in figures 11–15. In both cases the results for dense entry conditions, when the gate valve at the head of the chute is used to control the flow, are distinguished from those corresponding to loose entry conditions, when flow is controlled by the valve at the outlet of the feed hopper.

The observed behaviour is rather complex and is, perhaps, best explained by first describing a typical case, then indicating in what way the results differ for other cases. For this purpose we regard as typical the measurements on the smooth-based chute with inclinations of 15.5° or 16°, and in figure 3 a sketch of the $\dot{m}^*$ *vs* m_T^* relation for this case is supplemented by sketches of the velocity profiles at various

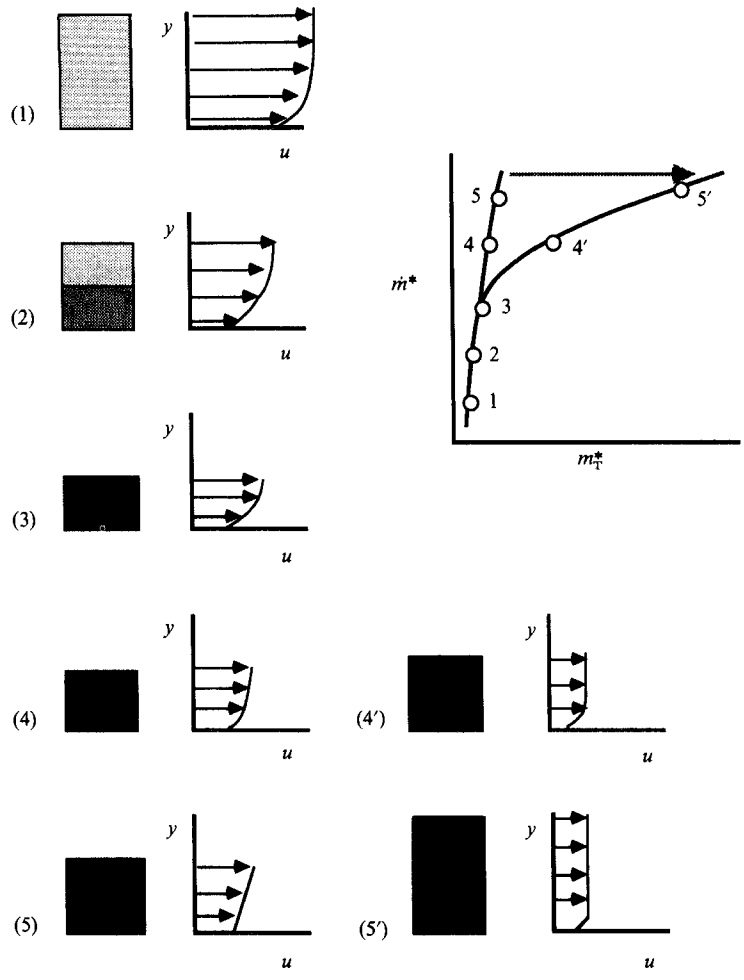

FIGURE 3. Summary of observed flow patterns.

identified points on the plot, each of which is accompanied by a small diagram in which the distribution of density through the flowing layer is indicated by density of shading.

At low values of $\dot{m}^*$ (point 1) the material flows as a diffuse, low-density layer, with particles occasionally bouncing quite high, so that the depth, as measured by the impact plate, is large. Velocities are high throughout the layer and, in particular, the slip velocity at the base of the chute is large. The fully developed flow appears to be the same for both loose and dense entry conditions, though the transient behaviour leading to it is different. With loose entry conditions the flowing layer decelerates and thickens, while with dense entry conditions it accelerates and becomes thinner while approaching the fully developed conformation.

When the flow rate is increased (point 2) a layer of markedly greater density forms above the base of the chute, with a diffuse layer of saltating particles, closely resembling the flowing layer at point 1, superimposed. The total depth, as determined by the impact plate, is smaller than at point 1, and velocities are lower. The larger value of the flow rate is, therefore, reflected in the increase of the average bulk density. Once again the fully developed flow appears to be independent of the

entry conditions. As $\dot{m}^*$ is increased the thickness of the dense sublayer increases, while the overall thickness decreases, so the dense layer occupies an increasing fraction of the depth. Velocities also decrease gradually, with decreasing slip velocity at the base plate.

With further increase in $\dot{m}^*$ (point 3) the diffuse saltating layer 'condenses' completely onto the dense layer, and velocities are again reduced. This point marks the boundary of operating conditions for which the fully developed flow is independent of entry conditions: for larger values of $\dot{m}^*$ there are two separate branches of the $\dot{m}^*$ *vs.* m_T^* curve, corresponding to dense and loose entry conditions, respectively. Following the curve for dense entry conditions beyond point 3, there is a sharp reduction in slope, the upper surface of the flowing layer becomes well defined, and the average density rapidly approaches a value corresponding to a solids volume fraction of approximately 0.6, near to random close packing. At the same time the velocity profile reveals that the rate of shear in the upper part of the layer becomes small, so the flow profile resembles that of a block of material near close packing, sliding without deformation on a thinner, shearing layer in contact with the base of the chute. There is a marked decrease in the velocities, and the increase in $\dot{m}^*$ is accounted for entirely by increases in the bulk density and the thickness of the flowing layer. These conditions correspond to point 4′ on the $\dot{m}^*$ *vs.* m_T^* plot.

As $\dot{m}^*$ is increased further, with dense entry conditions (point 5′), the layer remains almost close packed, its thickness increases rapidly, and the velocities become much smaller. Most of the material is now sliding with little deformation, and shearing is essentially confined to a relatively thin layer at the bottom. This type of flow is sustained up to the highest flow rates achievable, limited by the capacity of our recirculation system.

Turning now to the branch of the $\dot{m}^*$ *vs.* m_T^* curve representing flows generated from loose entry conditions, points 4 and 5 correspond to the same flow rates as points 4′ and 5′, respectively. As $\dot{m}^*$ is increased along this branch the average density increases continually and the thickness of the flowing layer also increases, but much more slowly than was the case for the dense entry condition branch. At the same time velocities decrease, but again not nearly so much as in the case of the other branch. At high values of the flow rate (point 5) the density of the flowing material has increased to a value similar to that at the corresponding point, 5′, on the other branch. Nevertheless, the two flows are very different. The thickness of the flowing layer at a point such as 5 on the loose entry branch is less than half that of the layer at the point 5′ of the dense entry branch, where the flow rate is the same, and correspondingly the velocities are more than twice as large. Furthermore, for points on the loose entry branch, the slip velocity at the base plate is relatively large and the velocity profile gives no indication of the presence of the 'locked', non-shearing layer below the free surface which was characteristic of the dense entry branch. There appears to be an upper bound for the flow rate on the loose entry branch. For higher feed rates the flow reverts to points on the dense entry branch, provided the inclination of the chute is steep enough for this branch to exist, and this is represented by the horizontal arrow in figure 3. The mechanism of this transition is interesting and will be described below.

We now consider the effect on this pattern of behaviour of changing the angle of inclination of the chute. The loose entry branches have steep slopes so, although $\dot{m}^*$ increases with the chute inclination for a given value of m_T^*, the position of the loose entry branch in the $(\dot{m}^*, m_T^*)$-plane is not much affected by changes in the inclination angle. On the other hand the inclination has a marked effect on the position of that

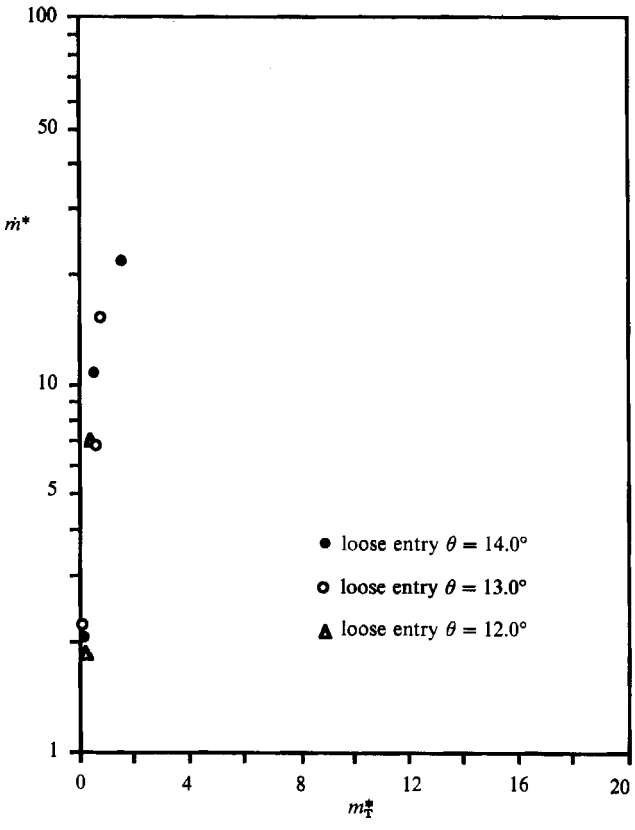

FIGURE 4. Observed relation between mass flow rate and mass hold-up for smooth chutes of inclinations 12°, 13° and 14°.

part of the dense entry branch that is separate from the loose entry branch. This is displaced upward with little change in slope as the inclination increases. As a consequence of these displacements of the separate branches, it is generally correct to conclude that their junction moves to higher values of $\dot{m}^*$ as the inclination is increased. However, this is masked, to some extent, by the intervention of other phenomena partly associated with the fact that the lengths of these branches are, in fact, bounded.

Considering first the loose entry branches, figure 4 shows observations of flows on these branches for small inclinations in the range 12° to 14°. In each case the branch is bounded above at a flow rate less than the limit imposed by the equipment, and the maximum attainable value of $\dot{m}^*$ increases with the inclination of the chute. For the values of the inclination on this figure steady flows cannot be established from dense entry conditions. The lowest value of the inclination is smaller than the angle of wall friction between a dense layer of the granular material and the base of the chute, so a dense layer rests quite immobile. For inclinations of 13° and 14° a dense layer can move, but the motion is of an irregular 'stick–slip' nature, and there is no steady flow. If an attempt is made, using loose entry conditions, to increase the flow beyond the indicated upper bound of the loose entry branch, the flowing layer collapses and there is either no flow at all, at 12° inclination, or stick–slip flow at the larger slopes.

At an inclination of 15° (figure 5) we first see steady flows developing from dense

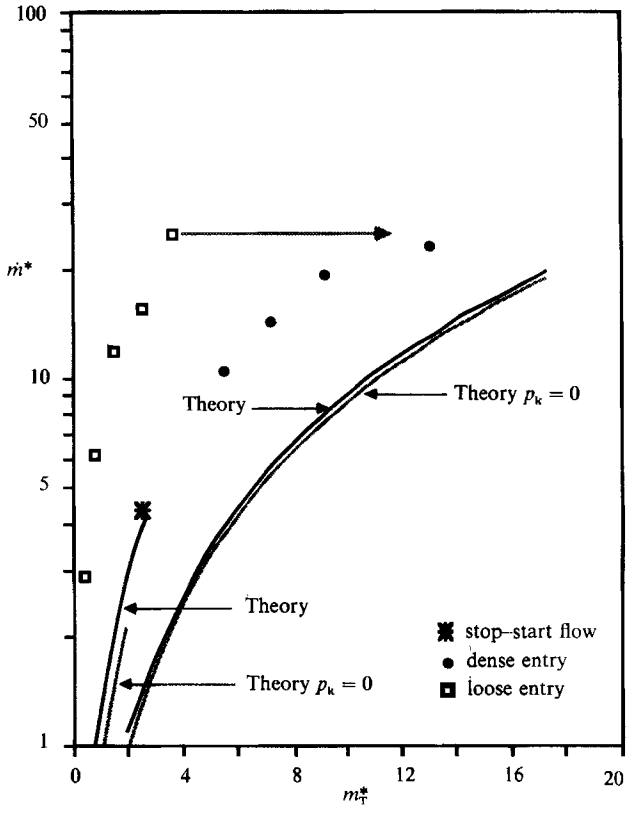

FIGURE 5. Observed and calculated relations between mass flow rate and mass hold-up for a smooth chute of inclination 15°.

entry conditions. However, these exist only for sufficiently large values of the flow rate. Below $\dot{m}^* = 10$ only stick–slip flow occurs, and below about $\dot{m}^* = 4$ no flow is possible with dense entry conditions. At this inclination, therefore, the intersection of the dense and loose entry branches, observed for slopes of 15.5° and above, as already described, is forestalled by the disappearance of the dense entry branch.

On the other hand, the existence of a dense entry branch at high flow rates provides a viable alternative mode of flow at the upper limit of the loose entry branch, and an increase in the feed rate at this point induces a jump to a point on the dense entry branch, as indicated by the horizontal arrow in figure 5. The mechanism of this transition is interesting. There is a sudden increase in the thickness of the layer and decrease in the velocity of the material at a point near the exit of the chute, then this change in thickness propagates upstream as a steep front separating the two modes of flow, until the whole chute is occupied by the deep, slow-moving layer that corresponds to the point on the dense entry branch. At an inclination of 15.5° (figure 6) the upper bound of the loose entry branch occurs near the maximum attainable flow rate, and more will be said about this case below. For inclinations larger than 15.5° the loose entry branch does not terminate within the range of the measurements, but we believe that the increase of its bound with increasing slope, observed at the lower inclinations, has simply carried it beyond the flow limit imposed by our equipment.

Comparing the results for 15.5° and 16° (figures 6 and 7) it is seen that the

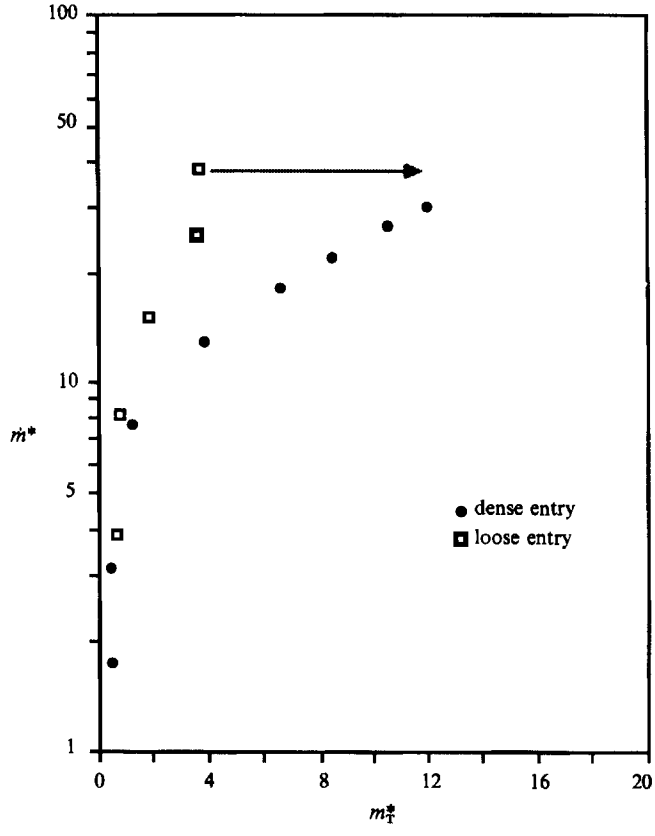

FIGURE 6. Observed relation between mass flow rate and mass hold-up for a smooth chute of inclination 15.5°.

intersection of the dense and loose entry branches moves upward as the inclination increases. However, at an inclination of 17° (figure 8) a new phenomenon appears. At low flow rates the loose and dense entry branches apparently coincide, as before, but on increasing the feed rate beyond about $\dot{m}^* = 33$, with dense entry conditions, there is a sudden and dramatic transition in which the depth of the flowing layer approximately doubles. This is indicated by an arrow pointing to the right in the figure. Further increases in flow rate then follow a dense entry branch, separate from the loose entry branch, with behaviour essentially the same as that observed at smaller inclinations. This branch can be retraced, as indicated by the open circles in the figure, and these extend well below the point at which the dense entry branch separated as the flow rate was increased. However, in this region oscillations of the free surface are observed, associated with small-amplitude surface waves travelling upstream from the chute exit at a speed estimated to be about 0.3 m/s. As the flow rate is decreased the amplitude of these oscillations increases until they apparently become large enough to trigger a second jump, leading back to the combined loose and dense entry branch. This is indicated by the arrow pointing back to the left in the figure. Apart from these transitions, and the hysteresis loop generated by them, the observed behaviour at a slope of 17° is similar to that at 15.5° and 16°.

The above oscillations may be related to those reported by Campbell *et al.* (1985) in relation to the transition between supercritical and subcritical flow. Indeed, the

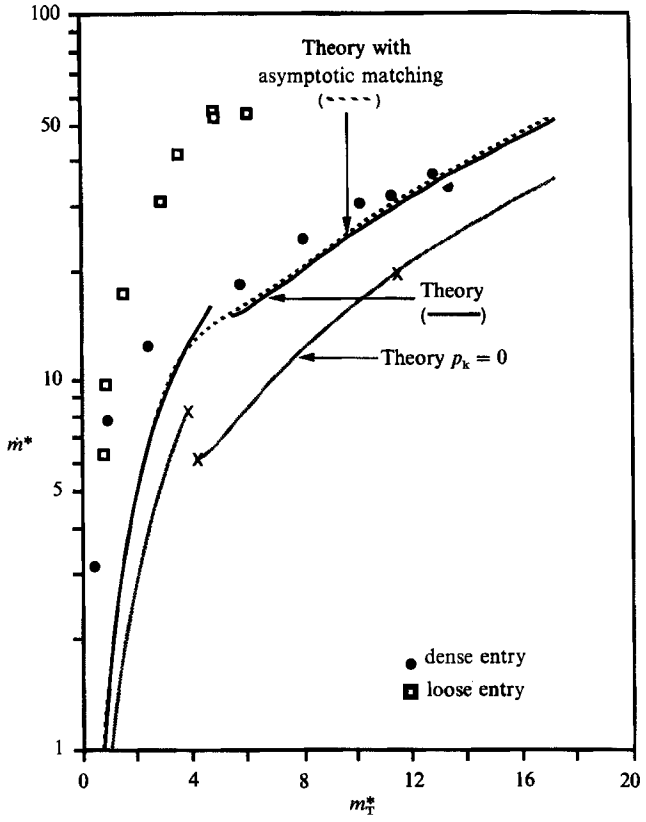

FIGURE 7. Observed and calculated relations between mass flow rate and mass hold-up for a smooth chute of inclination 16°. Crosses indicate points for which computed velocity profiles are shown in figure 17.

flowing layer on the dense entry branch just above the point of transition is subcritical, in their sense, while below the jump conditions are supercritical.

When the inclination is increased to 18° (figure 9) no branching phenomena are observed. Loose and dense entry conditions generate the same flows over the whole range of attainable feed rates. Nevertheless, we suspect that a separation of the branches would still be observed if it were possible to extend the conditions to higher flow rates. At inclinations larger than 18° there were clear indications that fully developed flow conditions had not always been reached in the available length of the chute, so no results are given for such slopes.

We appreciate the difficulty of being sure that acceleration is essentially complete in the flows we report as fully developed. In particular, the termination of the loose entry branches at some maximum value of the flow rate, and the nature of the transition which then occurs, suggests that flows on these branches may merely be extended transients that would always eventually decelerate to rest, or to one of the dense entry flows, given a chute of sufficient length. One might also suspect that the length required for this will depend on the kinetic energy of random motion of the particles when they enter the chute; that is, on the height from which they fall. However, in all the results reported here, the observed properties of the flowing layer were constant, within the accuracy of the measurements, from the midpoint of the chute on. Measurements of the free-surface centreline velocity were also made with

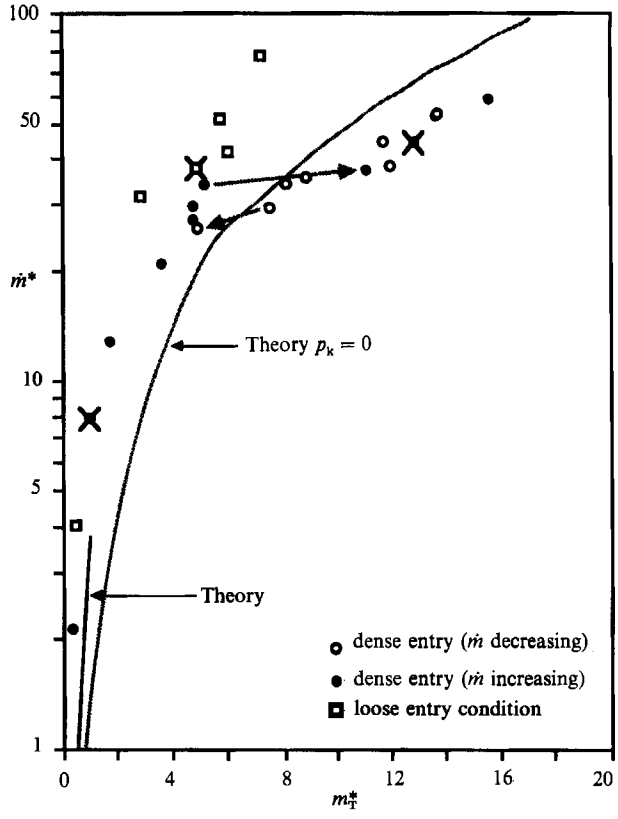

FIGURE 8. Observed and calculated relations between mass flow rate and mass hold-up for a smooth chute of inclination 17°. Crosses indicate points for which measured velocity profiles are shown in figure 10.

the fibre-optic probe, at points between 46 cm and 137 cm from the chute entrance and, within the measurement accuracy of 10%, this appeared to become constant before the chute exit, even for the loose branches at the highest flow rates. With dense entry conditions acceleration to the fully developed flow was apparently complete quite near the top of the chute. In summary then, we cannot exclude the possibility that the loose entry branches represent extended transients, but they persist for sufficient distances that, from the point of view of applications, this distinction may be unimportant.

Figure 10 shows a sample of measured velocity profiles for an inclination of 17°. These were taken 91.5 cm downstream from the chute entry, with the tip of the probe flush with the surface of the lateral wall. In figure 8 crosses identify the points corresponding to these measured profiles, and it is seen that two belong to the fast-moving branch, while the third is a slow, dense flow from well up the dense entry branch. The profiles are quite consistent with those sketched in figure 3 for corresponding conditions. It would be desirable to measure velocity profiles at the centreline, rather than the wall, but insertion of the fibre-optic probe more than 1 cm into the moving layer caused significant reduction in the flow rate, indicating an unacceptable perturbation of the flow.

The possibility of two different modes of flow for sufficiently high flow rates gives rise to an interesting phenomenon. As already described, at the upper bound of the

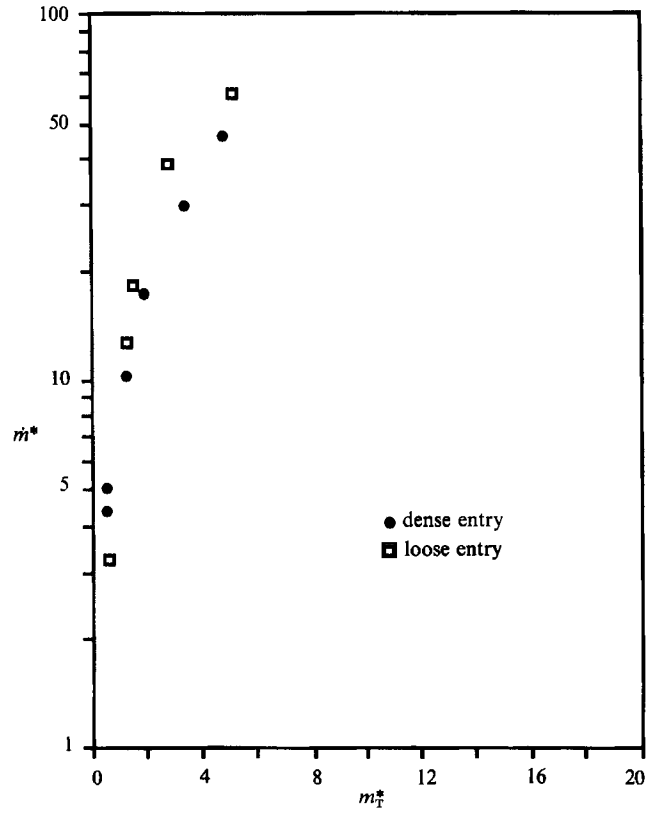

FIGURE 9. Observed relation between mass flow rate and mass hold-up for a smooth chute of inclination 18°.

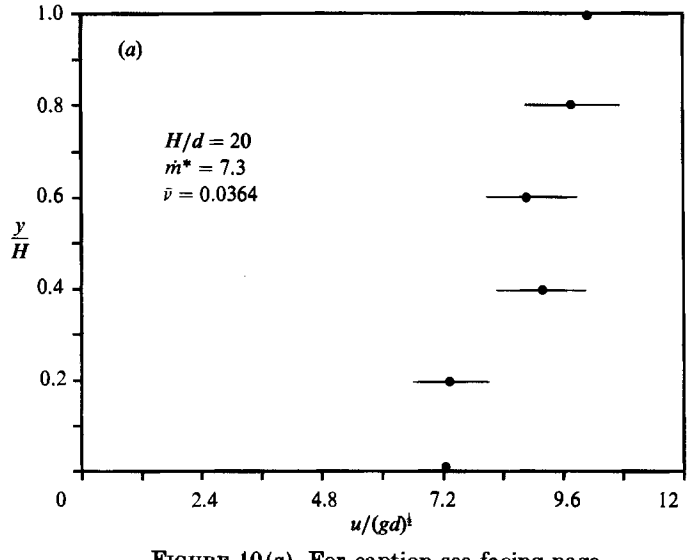

FIGURE 10(a). For caption see facing page.

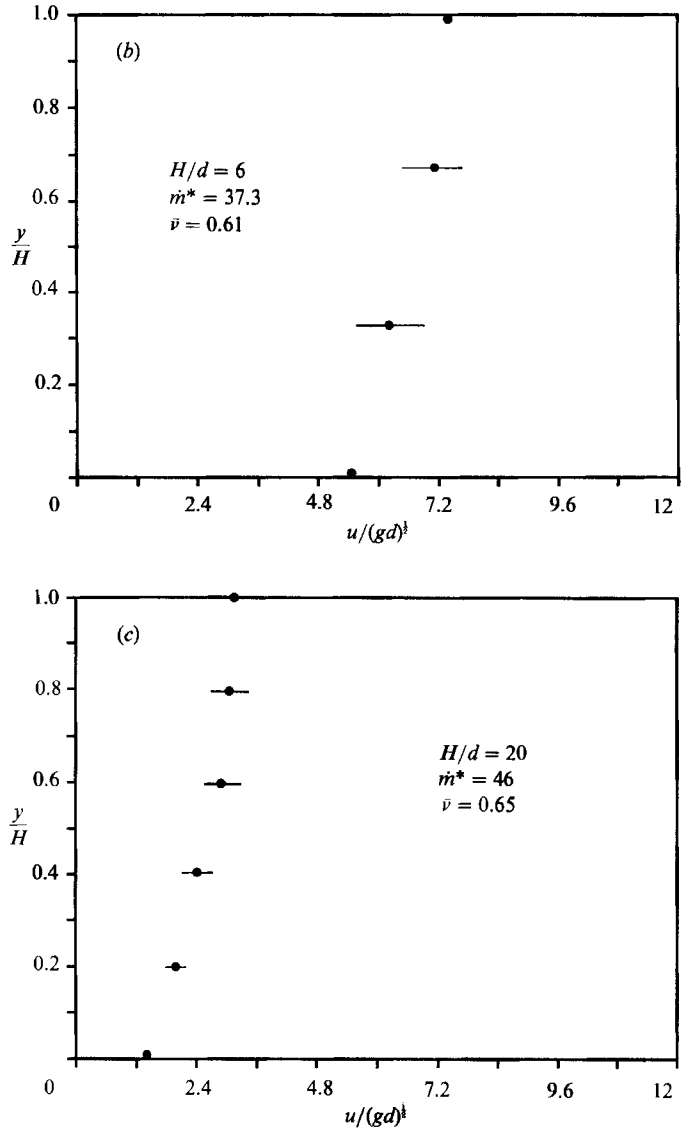

FIGURE 10. (*a–c*) Measured velocity profiles for a smooth chute of inclination 17°. Corresponding conditions are identified by crosses in figure 8.

loose entry branch a small increase in feed rate initiates a much slower, deeper flow at the chute exit, then this moves upward until it occupies the whole chute. However, if the feed rate is decreased slightly during this transition, it is possible to halt the upward progress of the front separating the two modes of flow. There is then a steady flow pattern with a shallow, fast flow belonging to the loose entry branch in the upper part of the chute, and a deep, slow flow belonging to the dense entry branch in the lower part. The two regimes are separated by a short transition region resembling a 'hydraulic jump' in the open channel flow of a liquid. But conventional hydraulic jumps form only upstream of some obstruction in the channel, while in the present case there is no obstruction.

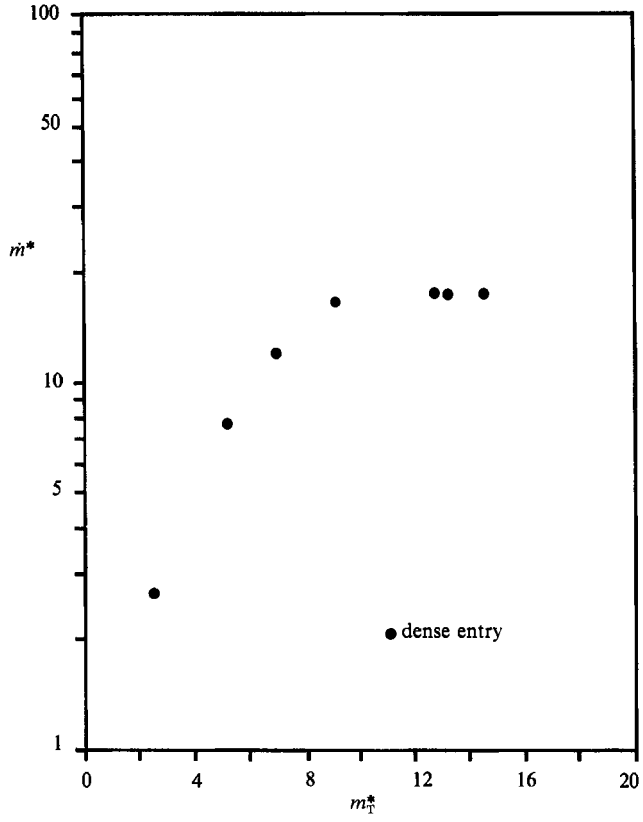

FIGURE 11. Observed relation between mass flow rate and mass hold-up for a rough chute of inclination 17°.

In addition to the work described above tests were also performed on a 'rough' chute, whose base plate was lined with 160-grit sandpaper. This presents a surface consisting of densely packed, immobile particles of angular shape, in the size range 100–200 μm. The resulting $\dot{m}^*$ *vs.* m_T^* plots, shown in figures 11–15, are generally similar to those found with the smooth chute. We shall therefore confine our comments mainly to the differences.

Steady flows are observed at larger inclination angles than in the case of the smooth chute, as might be expected, the range for the rough chute being 17° to 21°. At an inclination of 17° (figure 11) only dense entry condition flows are reported. With loose entry conditions the flow collapses into the dense entry mode before leaving the chute, over the whole range of feed rates tested. When the inclination is increased to 18° (figure 12) both loose and dense entry branches are found. These coincide at sufficiently low flow rates, and the loose entry branch is bounded above by a transition to the other branch, of just the same sort as was observed in the smooth chute. The pattern of behaviour is the same at 19° inclination (figure 13), but now both the branch point where the loose and dense entry branches separate, and the upper bound of the loose entry branch, occur at larger values of the flow. The dense entry branch also shows a small hysteresis, the black experimental points representing results obtained with successive increases in flow rate, while the open circles represent conditions observed when the flow rate is subsequently decreased in steps from its largest value. This hysteresis is quite reproducible. At an inclination

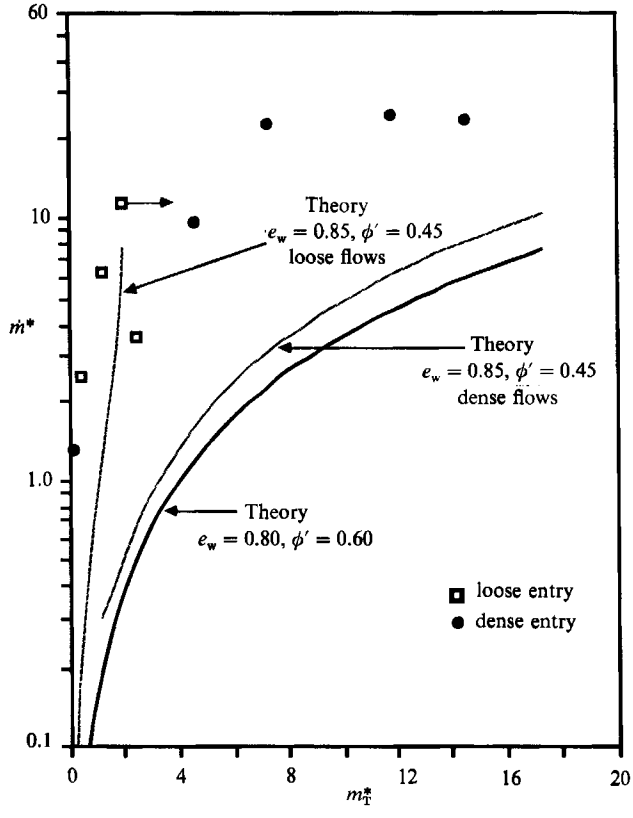

FIGURE 12. Observed and calculated relations between mass flow rate and mass hold-up for a rough chute of inclination 18°.

of 20° (figure 14) the separation of loose and dense entry branches occurs just below the maximum attainable flow rate, and when the slope is further increased to 21° (figure 15) the two branches coincide over the whole observed range.

In contrast to the case of the smooth chute, loose entry condition flows do not persist down to inclinations where dense flow is no longer possible. Instead the loose entry branch appears to be cut off by a rapid decrease in its upper bound at an inclination, namely 17° (figure 11), where dense entry flow is still possible. Another striking difference from the smooth chute is the absence of any jumps at the point of separation of the two branches, like those shown in figure 8. Correspondingly, oscillations of the surface of the flowing layer were never observed in the rough chute.

Other differences are quantitative. In the rough chute the loose entry condition branches for different inclinations lie so close together as to be almost indistinguishable if superimposed. Also, at the highest flow rates the dense entry branches flatten to very small slopes. This may correspond to an observation of Campbell (1982), who noted that there was a maximum flow rate per unit width at each value of the inclination. By varying the width of his chute Campbell found that this increased with increasing width, whereas the mass flow rate per unit width was independent of width for loose, fast flows.

Measurement of velocity profiles reveals another quantitative difference, which can be seen in the results for a slope of 20°, shown in figure 16. The corresponding conditions, both on the dense entry branch, are identified by crosses in figure 14. It

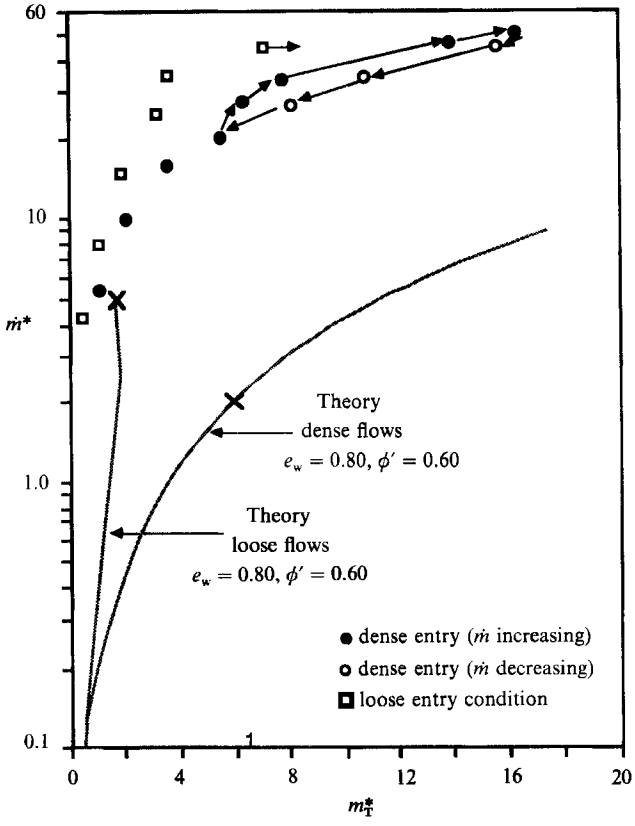

FIGURE 13. Observed and calculated relations between mass flow rate and mass hold-up for a rough chute of inclination 19°. Crosses indicate points for which computed velocity profiles and bulk densities are shown in figure 18.

is seen that there is little evidence of 'locking' of the upper layers in these flows; indeed, the velocity profiles are almost linear. This is, perhaps, to be expected in view of the larger resistance to slip at the base of the rough chute.

4.3. *Comparison with theoretical predictions*

Apart from α all the parameters in the theory are, in principle, directly measurable. Though we do not currently have the means to make all these measurements with adequate precision, we have attempted to base the values used on the best independent evidence available to us, and have made no attempt to vary them to secure a better match between theory and observations. There are two reasons for this. First, as remarked earlier, the theory is no more than a first attempt to combine features of both collisional and frictional contributions to the stress. The way this has been done is so simplistic that it is inconceivable it could generate quantitatively accurate predictions of behaviour. Its success should, therefore, be judged by the extent to which its predictions match the observed *pattern* of the observations over as wide as possible a range of operating conditions, using parameter values that are physically reasonable and consistent with such independent measures as are available. Second, any serious attempt to explore the effects of varying so large a set of parameters would be very time consuming and costly, and this must be set against the possibility of uncovering interesting varieties of behaviour within physically

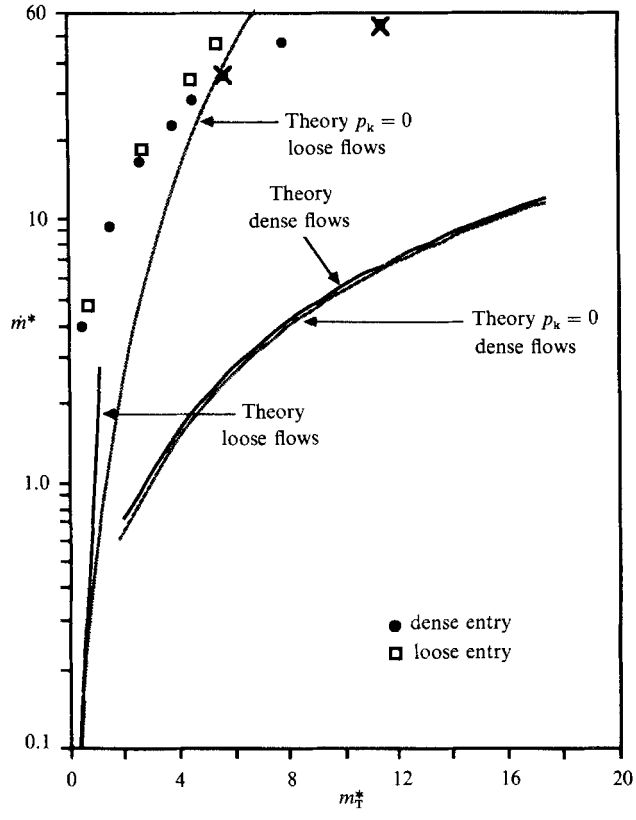

FIGURE 14. Observed and calculated relations between mass flow rate and mass hold-up for a rough chute of inclination 20°. Crosses indicate points for which measured velocity profiles are shown in figure 16.

realistic ranges of parameter values. In what follows we shall, therefore, first discuss the basis for our choice of parameter values, then compare the predicted and observed patterns of behaviour.

Properties of the glass beads needed for theoretical predictions are listed in table 2. The particle diameter and density are specified by the manufacturer and were checked by independent measurements. The internal angle of friction was measured with a Jenike-type shear tester, while the wall angle of friction was determined as the largest angle of inclination of the chute at which a layer of the beads several centimetres thick could rest without sliding. Angles of wall friction are quoted for both the smooth and the rough chute bases. No attempt was made to make separate measurements of friction at the sidewalls. Though the presence of these walls undoubtedly influences the quantitative results, the solution obtained here is one-dimensional, corresponding to a chute of infinite width. The coefficient of restitution for collisions between particles was estimated roughly by visual observation of the height of rebound of a particle from a glass plate, and the coefficient of restitution for particle–wall collisions was similarly found by observing rebounds from the base plate of the chute. The specularity coefficient is more difficult to measure, and reasonable values were simply assigned arbitrarily, with a relatively small magnitude for the smooth aluminium and a larger value for the sandpaper, from which rebounds are observed to scatter quite widely.

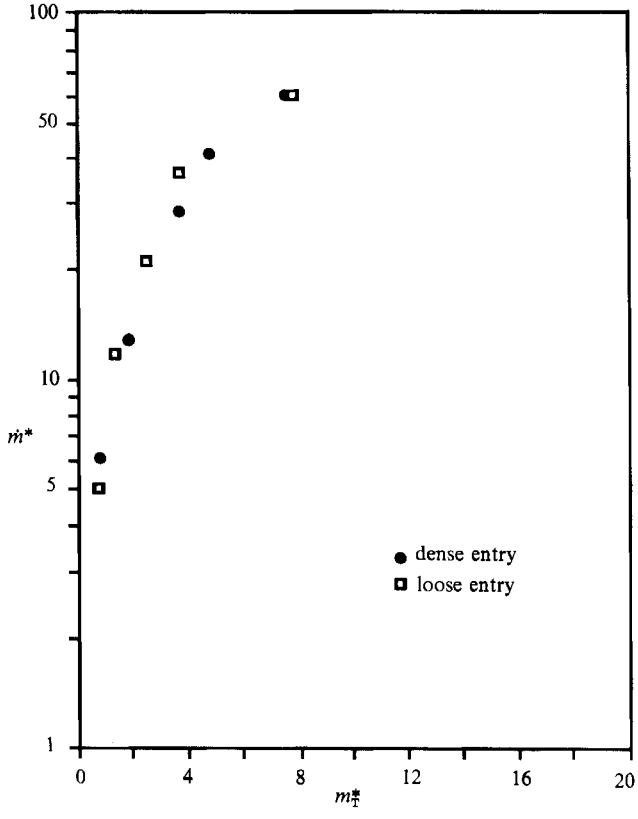

FIGURE 15. Observed relation between mass flow rate and mass hold-up for a rough chute of inclination 21°.

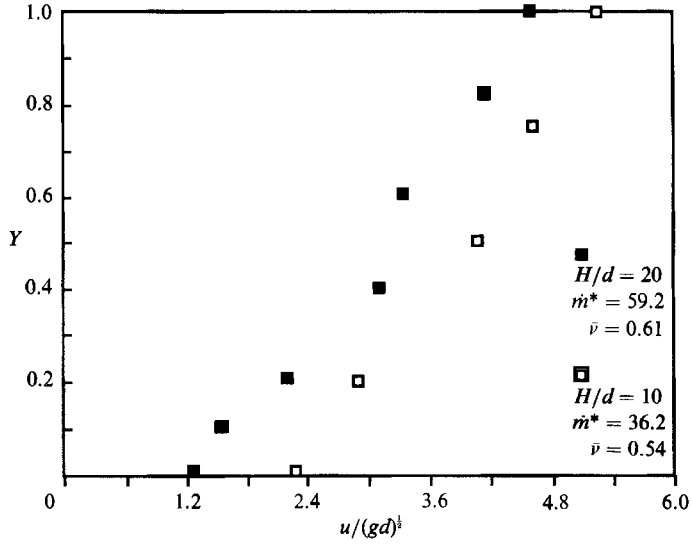

FIGURE 16. Measured velocity profiles for a rough chute of inclination 20°. Corresponding conditions are identified by crosses in figure 14.

d	particle diameter	0.10 cm
ρ_p	solids density	2.90 gm/cm^3
ϕ	internal angle of friction	28.5°
δ	wall angle of friction – smooth aluminium	12.3°
δ	wall angle of friction — 160 grit sandpaper	15.0°
e_p	grain–grain coefficient of restitution	0.91
e_w	grain–wall coefficient of restitution – smooth aluminium	0.91
e_w	grain–wall coefficient of restitution – 160 grit sandpaper	0.80
ϕ'	specularity coefficient – smooth aluminium	0.25
ϕ'	specularity coefficient – 160 grit sandpaper	0.60
$N_f(\nu)$	frictional normal stress at the critical state ($\nu \geqslant 0.50$) (gm/cm$-$s^2)	$0.5\dfrac{(\nu-0.50)^2}{(0.65-\nu)^5}$
α	constant appearing in $f_2(\nu)$	2.0

TABLE 2. Physical properties (the wall angle of friction δ is defined to be the angle below which no sliding is observed on an incline)

It remains to discuss the dependence of frictional normal stress on solids volume fraction, which was investigated by Scarlett & Todd (1969). For materials of our type their experiments indicate that N_f increases very rapidly as ν approaches ν_{max}, the maximum density of random packing. Their results shed no light on the form of N_f at very low normal loads, but it is reasonable to suppose that it will vanish for ν smaller than some value ν_{min}, at which the particles can no longer retain long-term contacts. We have therefore chose $n = 5$, $p = 2$, $\nu_{min} = 0.5$, and $\nu_{max} = 0.65$ in the normal stress equation (2.18). The multiplier Fr is then chosen so that $\nu = 0.58$ under a normal load equal to the weight of an overburden of a few centimetres of the particulate material. This is a typical value of ν for particles poured into a container under gravity.

Computed curves of $\dot{m}^*$ *vs.* m_T^*, both from the full theory and from the theory with $p_k = 0$, are shown for the smooth chute in figures 5, 7 and 8, corresponding to inclinations of 15°, 16° and 17°. In both versions of the theory the function $f_4(\nu)$, listed in table 1, was replaced by zero, which is equivalent to omitting the contribution to the energy flux proportional to the gradient of particle concentration. This affects the predicted mass flow rates by less than 1%.

The general shape of each curve is convex upward and quite steep at small values of m_T^*, and the ordinates increase progressively with the inclination. This corresponds well with the pattern found experimentally for the dense entry branches. At inclinations of 15° and 16° (figures 5 and 7) each curve consists of two branches, apparently separated by a discontinuity, and this discontinuity decreases in amplitude and shifts further up the curve when the inclination is increased. At an inclination of 17° (figure 8) there is no longer any discontinuity in the curve for $p_k = 0$, while solutions were found only for small values of $\dot{m}^*$ in the case of the full theory. Figure 17 shows computed velocity profiles at the points represented by crosses in figure 7. Across the discontinuity it is seen that shearing ceases at the surface and the uppermost layers of material 'lock up' into a block that slides without deforming. There is an increase in the mean density and a decrease in the mean velocity, but the latter dominates, and consequently the mass flow rate decreases. Beyond the discontinuity $\dot{m}^*$ resumes its increase with increasing m_T^*. It is likely that the computed curves are not actually discontinuous, but have intermediate branches joining the upper and lower branches shown in the diagrams.

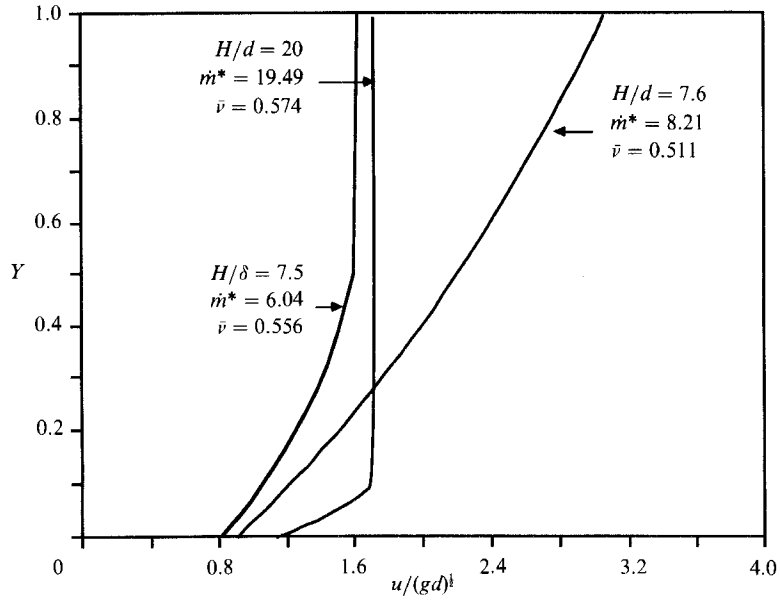

FIGURE 17. Computed velocity profiles for a smooth chute of inclination 16°. Theory with $p_k = 0$. Corresponding conditions are identified by crosses in figure 7.

However, we have not found a numerical procedure which converges to points on these branches. Recalling that our method of feeding particles to the chute effectively controls their flow rate, the presence of discontinuities in the theoretical curves may correspond to the jumps which are observed to occur in the neighbourhood of the point of separation of the loose and dense entry branches at an inclination of 17° (figure 8). Though the theory actually predicts discontinuities only for inclinations of 16° and below, this range could be changed by quite minor modifications in the parameter values.

The three computed velocity profiles shown in figure 17 illustrate very clearly the rapid development of 'lock up' on moving up the curves. The profile corresponding to the largest value of $\dot{m}^*$ shows most of the depth occupied by a sliding, rigid block of material riding on a relatively thin shearing layer. The experimental velocity profiles of figure 10, which correspond to the points distinguished by crosses in figure 8, again show the development towards a thick, slow-moving layer of material with little shear in its upper parts as the flow rate increases. Thus the observed pattern of change of the velocity profiles on moving along the ($\dot{m}^*$ m_T^*)-curve is reproduced by the theory.

Though the pattern of behaviour on the dense entry branches appears to have been modelled reasonably well the quantitative accuracy of predicted flow rates is not high, and it follows that good quantitative predictions of velocity profiles will not be obtained. As noted earlier, this is not to be expected at the present stage of development of the theory. However, at low flow rates the theory does not even give a qualitatively correct account of the flow, though this is not apparent from the plots of $\dot{m}^*$ *vs.* m_T^*. In this range the observed depth of the flowing layer decreases with increasing flow rate, while the theory predicts that it will increase. Furthermore, the theory predicts nothing resembling the dense sublayer which is observed to develop before the separation of the loose and dense entry branches as the flow rate is

increased. However, these remarks must be viewed in the light of what was said earlier about the difficulty of identifying a free surface at low flow rates, and in §5 we shall show that these qualitative shortcomings in the theory are most likely associated with the treatment of the free surface.

For the smooth chute in no case was anything resembling the loose entry branch predicted. The extension of the lower parts of the curves at the discontinuities might be regarded as the start of such a branch, but they do not extend nearly far enough to account for the observations. It is not clear whether this represents a real failure of the theory or whether, as suggested earlier, the extended loose entry branch observed experimentally is not truly a fully developed flow, but would revert to the dense entry branch in a long enough chute.

From table 2 it is seen that only the parameters δ, e_w and ϕ' must be changed to permit computations for the chute with the rough base, and the results of such computations are presented in figures 12, 13 and 14. For an inclination of 18° (figure 12), using the parameter values listed in table 2, the theory predicts a single curve relating $\dot{m}^*$ to m_T^*. At points on this curve the material is everywhere close to maximum density and the velocity profile is essentially flat. Thus the material is predicted to slide as a dense, rigid block, even at the lowest feed rates.

Results at 18° inclination are also presented for modified parameter values, $e_w = 0.85$ and $\phi' = 0.45$. These modest changes in the parameters induce a major qualitative change, namely the appearance of a discontinuity of the same type as those seen earlier in figures 5 and 7, but with a much larger jump separating the termini of the two branches. As before, the branch extending to large values of m_T^* represents a sliding block of material riding on a thin shear layer, while the other branch corresponds to much looser, faster flows. In view of its extended length it is tempting to identify this second branch with the observed flows generated from loose entry conditions. However, the predicted mean density of the flowing material decreases monotonically as $\dot{m}^*$ increases along this branch, while the measured density on the loose entry branch increases as the flow rate increases. At high flow rates, therefore, on this branch the theory predicts a diffuse flowing layer of low density, in contrast with the observation of a thin, dense layer. Consequently we must conclude that this theoretical branch does not represent any behaviour actually observed in our tests.

At an inclination of 19° (figure 13) two branches of solutions are found with the parameter values listed in table 2, and these retain the qualitative features described above for 18° slope. Two branches are also predicted for an inclination of 20°, as shown in figure 14, but the loose branch is now bounded above at quite a small value of $\dot{m}^*$. At this inclination results are also presented for the theory modified by setting $p_k = 0$. This has little effect on the dense branch, as might be expected since translational contributions are only a small proportion of the total stress, but the loose branch now extends to the largest value of $\dot{m}^*$ for which computations were performed, corresponding to a discontinuity of very large amplitude. As in the case of the smooth chute, we suspect that the curves for the rough chute are not actually discontinuous, but we have not succeeded in generating solutions corresponding to points on branches which would connect those plotted.

The quantitative predictions of $\dot{m}^*$ on the dense branches are very poor for the rough chute, though the pattern of behaviour in response to changes in flow rate and chute inclination is, once again, correctly represented. The predicted velocity and density profiles shown in figure 18 indicate that our choice of parameter values could be improved. These profiles correspond to conditions identified by crosses in figure

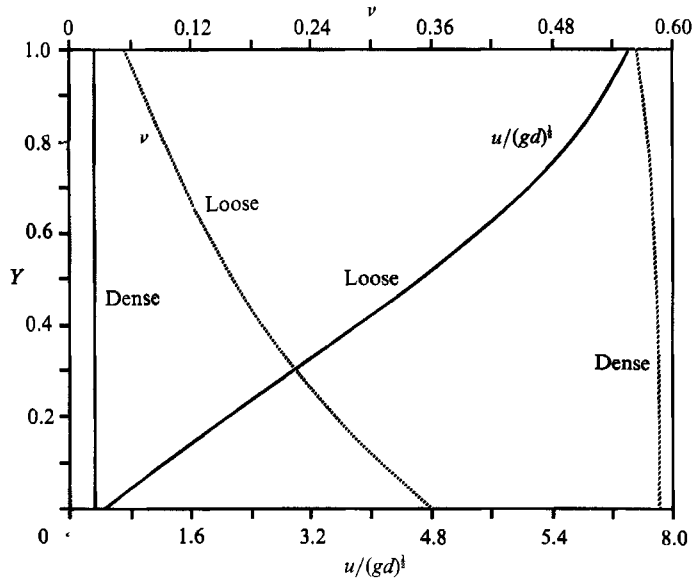

FIGURE 18. Computed velocity and bulk density profiles for a rough chute of inclination 19°. Dense entry flow: $\dot{m}^* = 1.8$, $H/d = 10$. Loose entry flow: $\dot{m}^* = 5.3$, $H/d = 10$. Corresponding conditions are identified by crosses in figure 13.

13, one on each of the branches. As noted earlier the dense solution is essentially a layer of maximum density sliding as a rigid block. There is much less evidence of the existence of a shearing layer in contact with the base than was found in the computations for the smooth chute presented as figure 17. In contrast, measured velocity profiles on a dense entry branch, shown in figure 16, exhibit shearing throughout the depth of the layer and little evidence of locking. It appears, therefore, that our choice of parameter values has led to underestimation of the energy input into the moving layer due to slip at its contact with the base of the chute. Consequently the layer is denser and less mobile than it should be, and the flow rate is smaller for a given mass hold-up.

5. A reconsideration of the free-surface boundary condition

At low feed rates our theoretical results predict an increase in depth of the flowing layer with increasing flow rate, while we observe that the depth actually decreases as the flow rate increases. This, and the failure to predict a loose entry branch with the observed behaviour, are the main qualitative shortcomings of the theory. However, at low flow rates the concept of a depth for the flowing layer is ambiguous, since the material is observed to flow as a diffuse cloud of saltating particles occasionally bouncing to considerable heights. In these conditions one is led to question whether the theoretical picture of the surface as a geometric plane, on which boundary conditions can be specified, is at all realistic. At high flow rates, on the other hand, the surface is observed to be well defined within one particle diameter, and the specification of free-surface boundary conditions seems entirely appropriate. We are thus led to ask whether the diffuse nature of the upper boundary at low flow rates and its sharp form at high flow rates ought not to be predicted, as consequences of a properly formulated theoretical description.

With this in mind we will reformulate the theory without the *a priori* concept of an upper surface. Instead we shall simply require that the bulk density should tend to zero with increasing height, derive asymptotic low-density solutions appropriate to describe the behaviour when the density becomes small, then match our numerical solutions to these at some sufficiently large height above the base. This process is then left to decide for itself whether or not there is a large change in density over a small distance, corresponding to a recognizable free surface.

5.1. *Matching to an asymptotic solution*

To be consistent with our earlier theoretical work we replace $f_4(\nu)$ by zero throughout in what follows. Taking the limiting forms of the functions f_1, f_2, f_3 and f_5 (table 1) as $\nu \to 0$, the equations of motion (3.1), (3.2) and (3.3) reduce to:

$$\frac{\partial}{\partial Y}[\nu T] = -\nu g \cos\theta, \tag{5.1}$$

$$\frac{\partial}{\partial Y}\left\{\frac{\beta T^{*\frac{1}{2}}}{A^{\frac{3}{2}}B^{\frac{1}{2}}}\frac{\partial u^*}{\partial Y}\right\} = -\nu, \tag{5.2}$$

$$\frac{\partial}{\partial Y}\left(\gamma T^{*\frac{1}{2}}\frac{\partial T^*}{\partial Y}\right) + AB\beta T^{*\frac{1}{2}}\left(\frac{\partial u^*}{\partial Y}\right)^2 - \omega A^2 T^{*\frac{3}{2}}, \tag{5.3}$$

where β and γ denote the limits of f_2 and f_3 respectively when ν tends to zero, f_5 is written as $\omega\nu^2$, and H, which is used to form the dimensionless coordinate Y, is now just an arbitrary scaling length to be determined later. When $y \to \infty$ we demand that $\nu \to 0$ and that the derivatives of u^* and T^* should both tend to zero, so that the stress and the flux of pseudo-thermal energy will both vanish. Thus, for large y, we write $u^* = u^*_\infty + u'^*$ and $T^* = T^*_\infty + T'^*$. Then ν, u'^* and T'^* are small far from the chute base, and all terms in the above equations (except the energy dissipation term, which would vanish) can be linearized in these variables. The resulting equations can then be solved explicitly, to give the following asymptotic forms for the solutions:

$$\nu(Y) = \nu^0 \exp\left(-\frac{A(Y-1)}{T^*_\infty}\right), \tag{5.4}$$

$$u^*(Y) = u^*_\infty - \frac{B^{\frac{1}{2}}T^{*\frac{3}{2}}_\infty \nu^0}{\beta A^{\frac{1}{2}}}\exp\left(-\frac{A(Y-1)}{T^*_\infty}\right), \tag{5.5}$$

$$T^* = T^*_\infty + \frac{\nu^{02}T^{*3}_\infty}{4\gamma}\left\{\omega - \frac{B^2}{\beta}\right\}\exp\left(-\frac{2A(Y-1)}{T^*_\infty}\right), \tag{5.6}$$

where ν^0 represents the value of ν at $Y = 1$.

In solving the equations of motion (3.1), (3.2) and (3.3), the boundary conditions (3.6), (3.7) and (3.8) at $Y = 1$ are now replaced by the requirement that the solution shall match, at $Y = 1$, the asymptotic solution given by (5.4), (5.5) and (5.6) above. Thus H becomes the height above the base at which the numerical and asymptotic solutions are matched. To start a numerical solution a value must be specified for H, thus determining the parameter A. Specification of $\nu(1)$, $u^*(1)$ and $T^*(1)$ then determines the values of ν^0, u^*_∞ and T^*_∞ from (5.4), (5.5) and (5.6) applied at $Y = 1$. Equations (5.5) and (5.6) can then be differentiated with respect to Y and, after setting $Y = 1$, they determine the first derivatives of u^* and T^* at this point. Since (3.1) is of the first order, while (3.2) and (3.3) are second order, initial conditions are

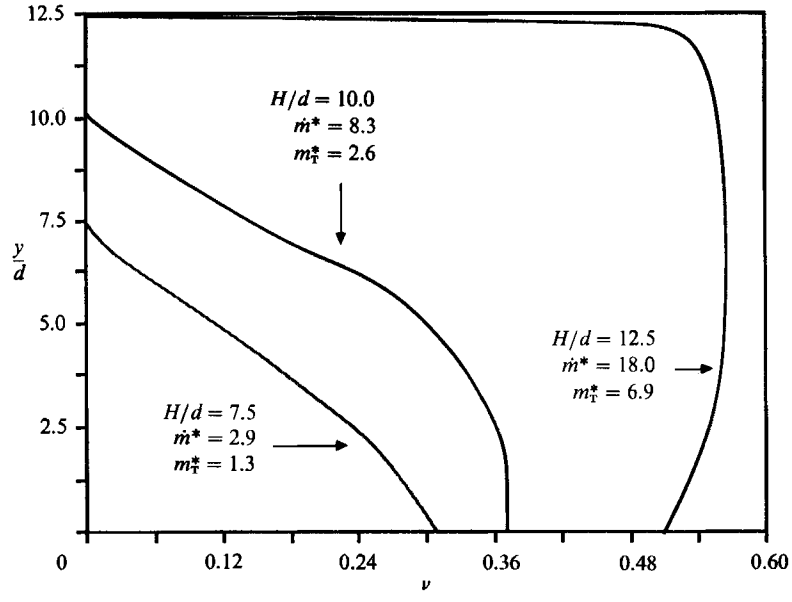

FIGURE 19. Theoretical bulk density profiles for a smooth chute of inclination 16°, obtained by matching to an asymptotic solution.

now available to initiate a numerical integration in the direction of decreasing Y, starting at $Y = 1$. This can be continued to $Y = 0$, where the boundary conditions (3.5) and (3.13) must be satisfied, and this requires iterative adjustment of the values of $u^*(1)$ and $T^*(1)$. Then there remain two parameters whose values are assignable, namely H and $\nu(1)$. However, by reverting to the dimensional form of the equations, it is easy to see that pairs $(H, \nu(1))$ and $(H', \nu'(1))$ correspond to different points on the same asymptotic solution if

$$\nu(1)\exp\left[\frac{Hg\cos\theta}{T_\infty}\right] = \nu'(1)\exp\left[\frac{H'g\cos\theta}{T_\infty}\right].$$

Thus, by varying H and making compensating changes in $\nu(1)$, as specified by this relation, the numerical solution can be matched to the same asymptotic solution at different heights above the base plate, thus checking that the result is not significantly affected by the matching height. The remaining freedom in the choice of these constants permits the one-parameter family of solutions for a given angle of inclination to be generated.

The numerical procedure actually used differs from this, in that it is formulated in terms of integrated forms of the momentum balances, and resembles that described in §3.2 sufficiently closely that further details need not be given here (see Johnson 1987). Convergence is slower than in the earlier calculations using free-surface boundary conditions, about a thousand iterations being needed to achieve comparable accuracy. Consequently a relatively small number of cases was studied. In figure 7 the $\dot{m}^*$ *vs.* m_T^* curve predicted in this way for an inclination of 16° is represented by a dotted line, and it is seen to differ little from the results found with a free-surface boundary condition. However figure 19, which shows computed density profiles at three points on this curve, has some new features. At the lowest feed rate, $\dot{m}^* = 2.9$, the bulk density is low and decreases steadily on moving up from

the base, and there is no very well-defined upper surface. When $\dot{m}^*$ is increased to 8.3 there is a region of quite high, and almost constant density immediately adjacent to the base, then a layer above this where the density decreases steadily. This is a new feature, not found with the free-surface boundary condition, and it appears to simulate the formation of the dense sublayer seen in the experiments. As also observed experimentally, the thickness of the predicted dense layer increases as the feed rate is increased, until a density profile like that shown for $\dot{m}^* = 18.0$ is obtained. This retains a high density up to a certain value of the depth, where there is a sudden decrease, so the theory now predicts the formation of a sharp upper surface, in agreement with the observed behaviour.

For each of the computed density profiles in figure 19 the numerical solution was matched to the asymptotic solution where $\nu = 0.001$. Though each of the curves appears to intersect the $\nu = 0$ axis at a finite value of y/d, the value of ν actually decreases exponentially as $y \to \infty$, as required by (5.4), and this decay is slowest for the lowest value of the feed rate. Thus, the curves cross as they approach the axis $\nu = 0$, and a diffuse low-density region extends to greater heights at the lower values of the feed rate. This is in qualitative agreement with the observation that the depth, as determined with the impact plate, decreases with increasing flow rate at small values of the flow rate. However, the predicted densities in this 'crossover' region are very low indeed.

6. Concluding remarks

In this and a previous paper (Johnson & Jackson 1987) we have explored some consequences of a constitutive model for granular materials which represents a first attempt to deal with situations where both frictional and collisional mechanisms of stress generation are significant. Our results indicate the importance of taking both mechanisms into account when dealing with flows in the Earth's gravity, in the absence of large, fixed overburdens. In these circumstances we have seen that either mechanism may dominate, and it is not uncommon for collisional and translational contributions to be the principal mechanism near a free surface, while frictional effects become predominant at quite modest depths. If either mechanism is omitted major qualitative features of the solutions are lost.

Our results also emphasize the importance of experimenters reporting fully the procedures by which their flows are initiated. In the case of plane shear of a horizontal layer discussed earlier (Johnson & Jackson 1987), this means that the sequence of operations used to prepare the sample and initiate the flow must be specified fully. In addition, for the case of chute flow treated here, the method used to feed the material into the chute must be specified, and the effects of changing this method should be explored.

The computed results are intended to illustrate the types of behaviour the model can predict. They in no sense represent a 'best fit' between theory and experiment, since only reasonable representative values of the parameters were used. The small number of calculations performed with alternative parameter values suffice to show that even the qualitative nature of the predicted behaviour can change in response to modest changes in the parameters. The qualitative behaviour of the dense entry branch is predicted well, even to such details as the discontinuous jumps seen in figure 8, the change in shape of the velocity profile on moving along the branch and, with the modified treatment of the free surface given in §5, the development of a relatively dense sublayer as the flow is increased from small values. However, the

quantitative accuracy of the predictions is poor. Though this might be improved by more precise experimental measurements of the parameters characterizing the particulate material, there are two obvious sources of error, one experimental and one theoretical. Experimentally, the observed flow in the chute is undoubtedly affected by the sidewalls, as can be seen from transverse velocity profiles at the free surface, but increasing the width of the chute would further restrict the range of conditions accessible within the capacity of our air lift. However, sidewall effects would be expected to decrease the observed flows, while in practice they are most often found to be larger than those predicted. Theoretically, as remarked in §4.3, because of the unrealistically simple way in which frictional and collisional contributions to the stress were identified separately, and combined additively, quantitative accuracy in prediction is not to be expected.

The main qualitative failure of the theory is the lack of second solutions representing the loose entry branch after it separates from the dense entry branch. (The second solutions found with modified parameter values for the rough chute have the wrong qualitative behaviour.) On the other hand, as noted earlier, it is possible that points on the separate part of the loose entry branch represent extended transients, rather than fully developed flows.

The quantitative accuracy of prediction remains poor even at low feed rates, where the density of the flowing material is low, collisional effects dominate, and the crude empiricism used in introducing frictional effects cannot be blamed. Of course, the collisional theory itself is by no means exact, and it is applied in a situation where departures from a Maxwellian velocity distribution are not small. However, it is more likely that problems arise from applying a theory derived for an infinite medium to a shearing layer that is both thin and dilute, so that collisions between particles and the base of the chute assume an importance comparable with interparticle collisions, as in the transition to Knudsen streaming of a gas. In the uppermost, and least dense part of the flowing layer the curvature of the free paths induced by gravity is also visibly marked.

This work is supported by the United States Department of Energy under Grant No. DE-FG22-86PC90518. It also forms part of a larger programme on various aspects of the motion of particulate systems, which is supported by the National Science Foundation, Multiphase and Interfacial Phenomena Program, under Grant No. CBT-8504201.

REFERENCES

AUGENSTEIN, D. A. & HOGG, R. 1978 An experimental study of the flow of dry powders over inclined surfaces. *Powder Technol.* **19**, 205–215.

BRENNEN, C. E., SIECK, K. & PASLASKI, J. 1983 Hydraulic jumps in granular material flow. *Powder Technol.* **35**, 31–37.

CAMPBELL, C. S. 1982 Shear flows of granular materials. PhD thesis, California Institute of Technology.

CAMPBELL, C. S., BRENNEN, C. E. & SABERSKY, R. H. 1985 Flow regimes in inclined open-channel flow of granular materials. *Powder Technol.* **41**, 77–82.

COULOMB, C. A. 1776 Essai sur une application des regles de maximis et minimis a quelques problemes de statique, relatifs a l'architecture. *Acad. R. Sci. Mem. Math. Phys. par Divers Savants* **7**, 343–382.

DRUCKER, D. C. & PRAGER, W. 1952 Soil mechanics and plastic analysis or limit design. *Q. Appl. Maths.* **10**, 157–165.

HAFF, P. K. 1983 Grain flow as a fluid-mechanical phenomenon. *J. Fluid Mech.* **134**, 401–430.

HUI, K., HAFF, P. K., UNGAR, J. E. & JACKSON, R. 1984 Boundary conditions for high-shear grain flows. *J. Fluid Mech.* **145**, 223–233.

HUTTER, K. & SHEIWILLER, T. 1983 Rapid plane flow of granular materials down a chute. In *Proc. US–Japan Seminar on New Models and Constitutive Relations in the Mechanics of Granular Materials* (ed. J. T. Jenkins & M. Satake). Elsevier.

ISHIDA, M. & SHIRAI, T. 1979 Velocity distributions in the flow of solid particles in an inclined open channel. *J. Chem. Engng Japan* **12**, 45–50.

JENKINS, J. T. & RICHMAN, M. W. 1985 Kinetic theory for plane flows of a dense gas of identical, rough, inelastic, circular disks. *Phys. Fluids* **28**, 3485–3494.

JENKINS, J. T. & RICHMAN, M. W. 1986 Boundary conditions for plane flows of smooth, nearly elastic, circular disks. *J. Fluid Mech.* **171**, 53–69.

JENKINS, J. T. & SAVAGE, S. B. 1983 A theory for the rapid flow of identical, smooth, nearly elastic, spherical particles. *J. Fluid Mech.* **130**, 187–202.

JOHNSON, P. C. 1987 Frictional–collisional equations of motion for particulate flows with application to chutes and shear cells. Ph.D. thesis, Princeton University.

JOHNSON, P. C. & JACKSON, R. 1987 Frictional–collisional constitutive relations for granular materials, with application to plane shearing. *J. Fluid Mech.* **176**, 67–93.

JONG, G. DE J. DE 1959 Statics and kinematics in the failable zone of granular material. Thesis, University of Delft.

JONG, G. DE J. DE 1977 Mathematical elaboration of the double-sliding free rotating model. *Arch. Mech.* **29**, 561–591.

LUN, C. K. K., SAVAGE, S. B., JEFFREY, D. J. & CHEPURNIY, N. 1984 Kinetic theories for granular flow: inelastic particles in Couette flow and slightly inelastic particles in a general flow field. *J. Fluid Mech.* **140**, 223–256.

MANDEL, J. 1947 Sur les lignes de glissement et le calcul des deplacements dans la deformation plastique. *C.R.Hebd. Sceanc. Acad. Sci. Paris* **225**, 1272.

PATROSE, B. & CARAM, H. S. 1982 Optical fiber probe transit anemometer for particle velocity measurements in fluidized beds. *AIChE J.* **28**, 604–609.

PATTON, J. S., BRENNEN, C. E. & SABERSKY, R. H. 1987 Shear flows of rapidly flowing granular materials. *Trans. ASME* E: *J. Appl. Mech.* **54**, 801–805.

REYNOLDS, O. 1885 On the dilatancy of media composed of rigid particles in contact. *Phil. Mag.* **20**, 469–481.

ROSCOE, K. H. 1970 The influence of strains in soil mechanics. *Géotechnique* **20**, 129–170.

ROSCOE, K. H., SCHOFIELD, A. N. & WROTH, C. P. 1958 On the yielding of soils. *Géotechnique* **8**, 22–53.

SAVAGE, S. B. 1978 Experiments on shear flows of cohesionless granular materials. In *Proc. US–Japan Seminar on Continuum-Mechanical and Statistical Approaches in the Mechanics of Granular Material*, pp. 241–254. Gakujutsu Bunken Fukyukai, Tokyo.

SAVAGE, S. B. 1979 Gravity flow of cohesionless granular materials in chutes and channels. *J. Fluid Mech.* **92**, 53–96.

SAVAGE, S. B. 1983 Granular flows down rough inclines – review and extension. In *Proc. US–Japan Seminar on New Models and Constitutive Relations in the Mechanics of Granular Materials* (ed. J. T. Jenkins & M. Satake). Elsevier.

SAVAGE, S. B. & JEFFREY, D. J. 1981 The stress tensor in a granular flow at high shear rates. *J. Fluid Mech.* **110**, 225–272.

SAVAGE, S. B. & SAYED, M. 1984 Stresses developed by dry cohesionless granular materials sheared in an annular shear cell. *J. Fluid Mech.* **142**, 391–430.

SCARLETT, B. & TODD, A. C. 1969 The critical porosity of free flowing solids. *Trans. ASME* B: *J. Engng Ind.* **91**, 477–488.

SCHOFIELD, A. N. & WROTH, C. P. 1968 *Critical State Soil Mechanics.* McGraw-Hill.